https://doi.org/10.1093/nar/gkab1098

The pioneer round of translation ensures proper targeting of ER and mitochondrial proteins

Joori Park[1,2,†], Jeeyoon Chang[1,2,†], Hyun Jung Hwang[1,2], Kwon Jeong[1,2], Hyuk-Joon Lee[2], Hongseok Ha[1,2], Yeonkyoung Park[1,2], Chunghun Lim[3], Jae-Sung Woo[2] and Yoon Ki Kim[1,2,*]

[1]Creative Research Initiatives Center for Molecular Biology of Translation, Korea University, Seoul 02841, Republic of Korea, [2]Division of Life Sciences, Korea University, Seoul 02841, Republic of Korea and [3]School of Life Sciences, Ulsan National Institute of Science and Technology, Ulsan 44919, Republic of Korea

Received May 02, 2021; Revised October 14, 2021; Editorial Decision October 19, 2021; Accepted October 21, 2021

ABSTRACT

The pioneer (or first) round of translation of newly synthesized mRNAs is largely mediated by a nuclear cap-binding complex (CBC). In a transcriptome-wide analysis of polysome-associated and CBC-bound transcripts, we identify RN7SL1, a noncoding RNA component of a signal recognition particle (SRP), as an interaction partner of the CBC. The direct CBC–SRP interaction safeguards against abnormal expression of polypeptides from a ribosome–nascent chain complex (RNC)–SRP complex until the latter is properly delivered to the endoplasmic reticulum. Failure of this surveillance causes abnormal expression of misfolded proteins at inappropriate intracellular locations, leading to a cytosolic stress response. This surveillance pathway also blocks protein synthesis through RNC–SRP misassembled on an mRNA encoding a mitochondrial protein. Thus, our results reveal a surveillance pathway in which pioneer translation ensures proper targeting of endoplasmic reticulum and mitochondrial proteins.

INTRODUCTION

Approximately 30% of newly synthesized proteins in eukaryotic cells are integral membrane proteins or secretory proteins, both of which should be transported to the surface or lumen of the endoplasmic reticulum (ER) (1). Accumulating evidence shows that selection of a protein destined for membrane integration or secretion proceeds co-translationally in the eukaryotic cell (2–7). As a nascent polypeptide chain emerges from the exit tunnel of an elongating ribosome, the N-terminal signal sequence composed of hydrophobic residues is co-translationally recognized by the signal recognition particle (SRP), which is pre-associated with the ribosome (8–11). The resulting complex composed of the ribosome–nascent chain complex (RNC) and the SRP is translationally arrested or delayed until it binds to the SRP receptor (SR), a heterodimer of SRα and SRβ located on the ER surface. Once the RNC–SRP complex is properly delivered to the ER, the SR binds to the SRP through heterodimerization of the NG domain (composed of a helical N-domain and a central GTPase domain) of SRP54 (a component of SRP) and the NG domain of SRα, triggering dissociation of SRP from the complex. The remaining RNC is then transferred to a translocon (Sec61 complex) (12) and eventually resumes translation elongation (2,3,7,11,13).

The mammalian SRP is composed of a single noncoding (nc) RNA (7SL RNA; RN7SL1) and six polypeptides, including SRP54, forming two functional domains (8–11). The Alu domain of SRP is involved in translational arrest of the RNC. The S domain recognizes the signal sequence in the RNC and binds to the SR in a GTP-dependent manner. In particular, the universally conserved SRP54 protein binds to the exit tunnel of the ribosome via its NG domain and recognizes the signal sequence through its methionine-rich M domain.

Due to the hydrophobic property of the N-terminal signal sequence, improper targeting of integral membrane proteins and secretory proteins often causes misfolding and/or aggregation of a nascent polypeptide and consequently induces proteotoxic stress (6,14–17). Therefore, to minimize mistargeting and aberrant synthesis of proteins destined for the ER, eukaryotic cells have evolved several quality control mechanisms operating at either mRNA or global levels (18). For instance, when an N-terminal signal sequence lacks a sufficient number of hydrophobic residues, the nascent chain in the RNC preferentially binds to Argonaute 2 (AGO2) rather than SRP (19). The mRNA in the resulting RNC–AGO2 complex is subjected to rapid degradation by unknown nuclease(s) in a process termed regu-

*To whom correspondence should be addressed. Tel: +82 2 3290 3410; Fax: +82 2 923 9923; Email: yk-kim@korea.ac.kr
†The authors wish it to be known that, in their opinion, the first two authors should be regarded as joint first authors.

lation of aberrant protein production (RAPP). In this way, the RAPP pathway selectively degrades mRNAs encoding aberrant signal sequences. An ER-associated protein degradation pathway and a regulated IRE-1–dependent mRNA decay pathway, which act as quality control mechanisms at the global level, are activated by the accumulating misfolded proteins in the ER, reducing global translation efficiency and levels of mRNAs encoding secretory proteins, respectively (18).

It is widely accepted that newly synthesized mRNAs being exported from the nucleus are largely subject to the pioneer (or the first) round of translation (pioneer translation) mediated by a nuclear cap-binding complex [CBC; a heterodimer of cap-binding proteins (CBPs) 80 and 20] (20,21). Pioneer translation is mostly involved in mRNA surveillance rather than active protein synthesis (20–22). For instance, an aberrant mRNA harboring a premature termination codon (PTC) is rapidly degraded by nonsense-mediated mRNA decay (NMD), the best-characterized mRNA surveillance mechanism (23,24), with most of the degradation occurring during pioneer translation (22). In contrast, when an mRNA is normal and thus passes the mRNA surveillance pathway during pioneer translation, a cytoplasmic cap-binding protein called eukaryotic translation initiation factor 4E (eIF4E) replaces the CBC with the help of importins (IMPs) α and β in a translation-independent manner (25–27). The resulting eIF4E-associated messenger ribonucleoprotein (mRNP) then participates in active protein synthesis.

In this study, we present compelling evidence for a CBC-ensured quality control pathway via which the CBC represses inadequate translation from the RNC–SRP complex until the complex is properly delivered to the ER.

MATERIALS AND METHODS

Plasmid construction

The following plasmids were used in this study: pCMV-Myc and pEGFP-C2 (Clontech); p3×FLAG-CMV™-7.1 (MilliporeSigma); pCMV-Myc-ER-GFP (Invitrogen); pCMV-Myc-GFP (28); pcDNA3-FLAG, pcDNA3-FLAG-CTIF, pcDNA3-FLAG-CBP80 and pmCMV-GPx1-Norm (29); pX (30); pCMV-Myc-eIF4E and pRβGl-SL0-Norm (31); pcDNA3.1-HA and pλN-HA-GFP (27); pCXbsr-mRFP-Ub and pCMV-Myc-GST (32); pMS2-HA-GFP (33); pCMV3-IMPβ-FLAG (Sino Biological; #HG17676-CF); pOTB7-SRP54, pCMV-SPORT6-SRα, pCMV-SPORT6-DPM3, pOTB7-PAM16, pCMV-SPORT6-SLC25A41 and pOTB7-ATP5F1E (ATP5E; Korea Human Gene Bank; hMU006286, hMU001253, hMU003974, hMU008804, hMU004511 and hMU005976, respectively); Lamp1-RFP (Addgene; #1817), mCh-Sec61β (Addgene; #49155); pcDNA3.1-FLAG-LC3B (a kind gift from Hyun Kyu Song, Korea University, Republic of Korea) and pWT-PPL-TET (19).

To construct plasmids pcDNA3-FLAG-CBP80(1–307), -CBP80(308–790) and -CBP80(664–790), the corresponding regions of human *CBP80* complementary DNAs (cDNAs) were PCR-amplified using pcDNA3-FLAG-CBP80 as the template and two specific oligonucleotides as primers: 5′-GACTACAAGGACGACGATGACAAGGCG-3′ (sense) and 5′-CCCAAGCTTTTAACTCCCTGGCA TGACAGGACCCTCGGG-3′ (antisense) for amplification of the 1–307 region; 5′-CGCGGATCCGATGTC AGTGGAAAGATTTGTAATAGAAGAG-3′ (sense) and 5′-TGATCAGCGGTTTAAACTTAAGCTTTTA-3′ (antisense) for amplification of the 308–790 region; and 5′-CGGGATCCGGAGAAACTTGCTAGGCAACACAA ACGG-3′ (sense) and the same antisense oligonucleotide that was used to amplify the 308–790 region for amplification of the 664–790 region. The underlined nucleotides specify the BamHI and HindIII restriction enzyme sites, respectively. Each PCR-amplified fragment was ligated to a BamHI/HindIII fragment of pcDNA3-FLAG.

To generate plasmid pcDNA3.1-CBP80-HA, the NheI/XhoI fragment of pcDNA3.1-HA was ligated to the NheI/XhoI fragment containing human *CBP80* cDNA, which was PCR-amplified using pcDNA3-FLAG-CBP80 as the template and two oligonucleotides as primers: 5′-CTAGCTAGCGCCACCATGTCGCGGCGGCGGC ACAGCGACGAGA-3′ (sense) and 5′-CCGCTCGAGCG GCCTGCAGGGCACAGAACTGCTGGAACA-3′ (antisense). The underlined nucleotides represent the NheI and XhoI restriction sites, respectively.

To construct plasmids pcDNA3.1-CBP80-L34E-HA, -L254E-HA and -L264E-HA, leucine at positions 34, 254 and 264 of CBP80 were replaced with glutamic acid. Then, pcDNA3.1-CBP80^{R}-WT-HA and CBP80^{R}-L34E-HA plasmids expressing an siRNA-resistant (R) version of CBP80-WT-HA and CBP80-L34E-HA, respectively, were generated by changing the specific target sequences annealing to *CBP80* siRNA from 5′-GGAAGAAGCUAAAGAGAAA-3′ to 5′-AGAGGAGGCAAAGGAAAAG-3′, where the underlined nucleotides represent the silent mutation sites that confer resistance to *CBP80* siRNA.

To generate pcDNA3.1-CBP80-(23–790)-HA encoding the N-terminal deletion mutant of CBP80 that does not interact with IMPα (26), the NheI/ApaI fragment of pcDNA3.1-HA was ligated to a PCR product amplified from pcDNA3-FLAG-CBP80 template using the oligonucleotides: 5′-CTAGCTAGCGCCACCATGGAT GCAAATGAAACTGAAGATCATTTGG-3′ (sense) and 5′-TTAGGATGTGCCGTTCCTGCCAGCGATC-3′ (antisense) as primers. The underlined nucleotides specify the NheI restriction site.

To construct the plasmid pcDNA3.1-SRP54-HA encoding full-length human *SRP54* cDNA, the NheI/XhoI fragment of pcDNA3.1-HA was ligated to the PCR-amplified NheI/XhoI fragment containing *SRP54* cDNA. PCR was carried out using pOTB7-SRP54 as the template and two oligonucleotides as primers: 5′-CTGGCTAGCGCCACC ATGGTTCTAGCAGACCTTGGAAG-3′ (sense) and 5′-TGGCTCGAGTCATATTATTGAATCCCATCATG-3′ (antisense), where the underlined nucleotides denote the NheI and XhoI restriction sites, respectively.

To construct p3 × FLAG-SRP54-FL, -NG and -M, the corresponding regions of human *SRP54* cDNA were amplified by PCR, using pOTB7-SRP54 as the template and specific oligonucleotides as primers: 5′-

CGGGGTACCAATGGTTCTAGCAGACCTTGGAAG-3′ (sense for FL and NG), 5′-CGGGGTACCAATG CTTCTTGGTATGGGCGACATTG-3′ (sense for M), 5′-TCCCCCGGGTTACATATTATTGAATCCCATCAT GC-3′ (antisense for FL and M), and 5′-TCCCCCGGGTT ATTTGCTAATAAAAGGCTGTGTTTTG-3′ (antisense for NG). The underlined nucleotides specify KpnI and SmaI restriction sites, respectively. Each PCR-amplified fragment was ligated to the KpnI/SmaI fragment of p3×FLAG.

To generate plasmids pCMV-Myc-SRα-SRX and -NG, the corresponding regions of human *SRα* cDNA were PCR-amplified using pCMV-SPORT6-SRα as a template and the following specific oligonucleotides: 5′-ACGCGTCGACCATGCTCGACTTCTTCACCATT TTCTCCAAG-3′ (sense for SRX), 5′-CGGGGTACCTT ACTTGGTCGCACTAGGTTTGGTAGAGTTTTG-3′ (antisense for SRX), 5′-ACGCGTCGACCGGAACAC TGGGTGGCATGTTTGGTATGCTG-3′ (sense for NG), and 5′-CGGGGTACCTTAAGCCTTCATGA GGGCAGCCACCACAGC-3′ (antisense for NG). The underlined nucleotides represent SalI and KpnI sites, respectively. Each PCR-amplified fragment was ligated to the SalI/KpnI fragment of pCMV-Myc.

To construct pX-CBP80-eYFP-10×His, which encodes human CBP80 fused to the C-terminus of 10×His-tagged enhanced yellow fluorescent protein (eYFP), the eYFP-10×His sequence was inserted into the pX vector. Then, a PCR-amplified fragment containing *CBP80* cDNA was inserted at a SalI restriction site upstream of eYFP-10×His. PCR was performed using pcDNA3-FLAG-CBP80 as the template and two oligonucleotides: 5′-ACGCGTCGACAT GTCGCGGCGGCGGCACAGCGACGAGAAC-3′ (sense) and 5′-GCCGACGTCGACGGCCTGCAGGGC ACAGAACTGCTGGAACAC-3′ (antisense), where the underlined nucleotides denote the SalI restriction site.

To construct pX-CBP20-Protein G, which encodes human CBP20 fused at the C-terminus of protein G, the protein G sequence was inserted into the pX vector. Next, a PCR-amplified fragment containing *CBP20* cDNA was inserted at SalI and XbaI sites upstream of the protein G gene. PCR was carried out using a plasmid harboring human *CBP20* cDNA (29) as the template and two oligonucleotides: 5′-ACGCGTCGACATGT CGGGTGGCCTCCTGAAGGCGCTGCGC-3′ (sense) and 5′-TGCTCTAGACTGGTTCTGTGCCAGYYY YCCATAGCCTCC-3′ (antisense), where the underlined nucleotides specify the SalI and XbaI restriction sites, respectively.

To generate pXFlagR-SRP54-NG for the purification of recombinant protein on the α-Flag M1 antibody resin (MilliporeSigma), a sequence containing 10×His-FLAG-multicloning site-mCherry-10 × His was inserted into pX. Next, the PCR-amplified DNA fragment corresponding to the N-terminal segment of human SRP54 (residues 1–293; SRP54-NG) was inserted into the multicloning sites (XhoI/XbaI sites). PCR was conducted using p3×FLAG-SRP54-NG as the template and specific oligonucleotides: 5′-CCGCTCGAGATGGTTCTAGCAGACCTTGGAAG-3′ (sense) and 5′-TGCTCTAGATTTGCTAATAAAAG GCTGTGTTTTG-3′ (antisense), where the underlined nucleotides represent the XhoI and XbaI restriction sites, respectively.

To construct pcDNA3-FLAG-GFP, the BamHI/HindIII fragment of pcDNA3-FLAG was ligated to a PCR-amplified fragment containing the full-length GFP cDNA that was digested with BamHI and HindIII. The *GFP* cDNA was amplified from a pEGFP-C2 template using two oligonucleotides: 5′-CGGGATCCGCTCGAGATG GTGAGCAAGGGCGAGGAGCTGTTC-3′ (sense) and 5′-CCCAAGCTTGCGGCCGCCTACTTGTACAGCT CGTCCATGCCGAGAGTG-3′ (antisense), where the underlined nucleotides specify the BamHI and HindIII sites, respectively.

To generate plasmids pCon-RβGl and pPPL-RβGl, the 5′ untranslated region of pRβGl-SL0-Norm was replaced with a fragment harboring either Con or PPL sequences, respectively, obtained from pWT-PPL-TET.

To construct pCon-FLAG-GPx1 and pPPL-FLAG-GPx1, we first generated p3×FLAG-GPx1 by inserting a *GPx1* genomic sequence (obtained from pmCMV-GPx1-Norm) into p3xFLAG. Then, Con and PPL sequences obtained from pCon-RβGl and pPPL-RβGl, respectively, were inserted immediately upstream of the FLAG sequence of p3 × FLAG-GPx1.

To construct pCMV-DPM3-GFP, pCMV-PAM16-GFP, pCMV-SLC25A41-GFP and pCMV-ATP5E-GFP (which encode either the ER- or mitochondria-targeted protein), the Myc sequences in pCMV-Myc-GFP were replaced with full-length cDNA sequences of human *DPM3*, *PAM16*, *SLC25A41* or *ATP5E*, respectively.

To construct pλN-HA-GST, the XbaI/NotI fragment of pλN-HA-GFP was ligated to a PCR-amplified DNA fragment encoding full-length GST that was digested with XbaI and NotI. The GST sequence was PCR-amplified from a pCMV-Myc-GST template using two oligonucleotides: 5′-GCTCTAGAGATGGCCCCTATAC TAGGTTATTGGAAAATTAAG-3′ (sense) and 5′-CTG CATTCTAGTTGTGGTTTGTCCAAACTCATC-3′ (antisense), where the underlined nucleotides specify the XbaI site.

All PCRs were carried out using the Advantage-HF2 PCR Kit (Clontech). All constructs were verified by sequencing.

Cell culture

HeLa (female; ATCC), HEK293T (fetal; ATCC), HEK293-EBNA (fetal; ATCC) and HEK293FT cells (fetal; ATCC) were maintained in Dulbecco's modified Eagle's medium (DMEM; Capricorn Scientific) supplemented with 10% fetal bovine serum (Capricorn Scientific) and 1% penicillin/streptomycin (Capricorn Scientific). To prevent mycoplasma contamination, all cultured cells were regularly treated with Plasmocin™ (Invivogen) and analyzed using the MycoAlert PLUS Mycoplasma Detection Kit (Lonza).

For heat shock experiments, HeLa cells were subjected to heat shock treatment by incubating at 42°C for 30 min and recovery at 37°C for different periods.

DNA or siRNA transfection

Cells were transiently transfected with various plasmids using either calcium phosphate method or Lipofectamine 2000 (Thermo Fisher Scientific), as described previously (33,34).

For siRNA transfection, the cells were transfected with 100 nM *in vitro*-synthesized siRNAs (GenePharma) using either Oligofectamine (Thermo Fisher Scientific) or Lipofectamine 3000 (Thermo Fisher Scientific), as described previously (33,34). The following siRNA sequences were used for specific downregulation of endogenous proteins: 5′-r(AAAUUUGGUAAGAACAAUG)d(TT)-3′ (*SRα* siRNA), 5′-r(UAUUGUUGACUCUGUAUAC)d(TT)-3′ (*SRβ* siRNA), 5′-r(GGAAGAAGCUAAAGAGAAA)d(TT)-3′ (*CBP80* siRNA), 5′-r(CAGGUUGUUCAUAGUCAGAAU)d(TT)-3′ (*HSF1* siRNA), and 5′-r(ACAAUCCUGAUCAGAAACC)d(TT)-3′ (nonspecific control siRNA).

RNA preparation, reverse transcription PCR (RT-PCR) and quantitative RT-PCR (qRT-PCR)

Details of RNA preparation, cDNA synthesis, and RT-PCR analyses have been described elsewhere (33,34). Briefly, total cell RNA isolated using TRIzol Reagent (Life Technologies) was subjected to DNA digestion using 0.05 U/μl DNase I (Thermo Fischer Scientific) at 37°C for 45 min. Purified RNA was incubated with 6 U/μl RevertAid reverse transcriptase (Thermo Fisher Scientific) at 37°C for 2 h. After the reaction, qRT-PCR was conducted using the reverse-transcribed cDNA, gene-specific oligonucleotides (Supplementary Table S1), and the LightCycler 480 SYBR Green I Master Kit (Roche), as described previously (33,34). qRT-PCR analysis was performed according to the MIQE guidelines (35).

Western blotting, immunoprecipitation (IP) and RNA-immunoprecipitation (RNA-IP) assays

Antibodies against the following proteins were used for western blotting or IP: CBP80 (36), eIF4E [cat. # 2067, Cell Signaling Technology (rabbit), or cat. # 610269, BD Biosciences (mouse) for western blotting], eIF3b (sc-16377, Santa Cruz Biotechnology), β-actin (A5441, MilliporeSigma), eIF4GI (29), IMPα (A300-484A, Bethyl Laboratories), SRP72 (NBP1-89498, Novus Biologicals), SRP68 (11585–1-AP, Proteintech), SRP54 (610940, BD Biosciences), SRP19 (16033-1-AP, Proteintech), SRP9 (11195-1-AP, Proteintech), SRα (H00006734-B02P, Novus Biologicals), SRβ (NBP2-02028, Novus Biologicals), p53 (2524, Cell Signaling Technology), Y14 (MAB2484, Abnova), MAGOH (ab38768, Abcam), DCP1A (D5444, MilliporeSigma), G3BP1 (13057-2-AP, Proteintech), HSF1 (4356, Cell Signaling Technology), phospho-Ser326-HSF1 (ab76076, Abcam), FLAG (α-DYKDDDDK, 14793, Cell Signaling Technology or A8592, MilliporeSigma), Myc (9E10; OP10L, MilliporeSigma), GFP (sc-9996, Santa Cruz Biotechnology) and HA (11867431001, Roche). For all eIF4E IP assays except the experiment in Figure 1A and Supplementary Figure S1A and B, we used an in-house α-eIF4E antibody (27). The IP assays depicted in Figure 1A and Supplementary Figure S1A and B were carried out using a commercial α-eIF4E antibody (sc-9976, Santa Cruz Biotechnology).

The following secondary antibodies were used for western blotting: horseradish peroxidase (HRP)-conjugated goat α-mouse IgG antibody (AP124P, MilliporeSigma), HRP-conjugated goat α-rabbit IgG antibody (AP132P, MilliporeSigma), HRP-conjugated rabbit α-goat IgG antibody (A5420, MilliporeSigma) and HRP-conjugated goat α-rat IgG antibody (ab6845, Abcam).

IP and RNA-IP assays were performed as previously described (33,34). Where indicated, the cells were treated with 3.7% formaldehyde (Millipore Sigma) in phosphate-buffered saline (PBS) for 10 min. Bead-bound proteins and mRNAs were assayed using western blotting and qRT-PCR, respectively.

Signal intensities of western blot bands were quantitated using ImageJ software (version 1.5, National Institutes of Health).

Recombinant protein purification

To purify the CBC, HEK293-EBNA cells were transiently co-transfected with two plasmids: pX-CBP80-eYFP-10×His and pX-CBP20-Protein G. Dimethyl sulfoxide (Amresco) was added immediately after the transfection to get a final concentration of 1%, and the temperature was lowered to 33°C. Two days after transfection, tryptone (Amresco) was added to get a final concentration of 0.5%. Three days after transfection, the cells were harvested and resuspended in buffer A [20 mM Tris–HCl (pH 7.5), 250 mM NaCl, and 2 mM β-mercaptoethanol] supplemented with 10% glycerol, 2 μg/ml staphylococcal nuclease, 5 mM $CaCl_2$, 1 mM PMSF and one tablet of EDTA-Free Pierce™ Protease Inhibitor Tablets (Thermo Fisher Scientific). The resuspended cells were lysed by sonication. The supernatant was separated by centrifugation, loaded onto a Ni-NTA column (Qiagen), and washed with buffer A supplemented with 40 mM imidazole (MilliporeSigma). Bound proteins were eluted with buffer A supplemented with 200 mM imidazole. The eluted proteins were then loaded onto a HiTrap™ Q HP column (GE Healthcare) equilibrated with a buffer consisting of 20 mM Tris–HCl (pH 7.5), 100 mM NaCl, and 2 mM β-mercaptoethanol. The column-bound proteins were eluted using a NaCl gradient of 100–500 mM. The fractions containing the CBC were collected and treated overnight with His-tagged human rhinovirus 3C protease to cleave the junctions between CBP80 and eYFP-10×His and between CBP20 and protein G. Each protease-treated sample was loaded onto the Ni-NTA column again to remove His-tagged proteases, eYFP-10×His, and other protein impurities with substantial Ni-binding affinity. Approximately half of the CBC proteins passed through the column, while the other half bound weakly to the resin and were eluted using buffer A supplemented with 20 mM imidazole. The flow-through and eluted fractions were pooled, concentrated to 1.7 mg/ml, and then purified further using a HiLoad 16/600 Superdex 200 pg column (GE Healthcare) equilibrated with buffer B [20 mM Tris–HCl (pH 7.5), 250 mM NaCl, and 2 mM dithiothreitol]. The peak fraction

(0.6 mg/ml) was flash-frozen in liquid nitrogen and stored at −80°C.

To purify FLAG-SRP54-NG, HEK293-EBNA cells grown in suspension were transiently transfected with pXFlagR-SRP54-NG. SRP54-NG was expressed as a fusion protein with the 10×His-FLAG tag at the N-terminus and the mCherry-10×His tag at the C terminus. The protein was produced using a protocol similar to that described for CBC purification. The cell extract was loaded onto a Ni-NTA column. Eluted proteins were treated overnight with tobacco etch virus protease and HRV 3C protease to expose the FLAG tag at the N-terminus and to remove the C-terminal mCherry-10×His, respectively. The sample was mixed with α-FLAG M1 agarose resin (MilliporeSigma) in the presence of 5 mM $CaCl_2$ under slow rotation at 4°C for 1 h. After washing with buffer A supplemented with 1 mM $CaCl_2$, bound proteins were eluted using buffer A supplemented with 5 mM EGTA. The eluted FLAG-SRP54-NG was concentrated to 0.2 mg/ml and further purified using a HiLoad 16/600 Superdex 200 pg column equilibrated with buffer B. The peak fraction was concentrated to 0.4 mg/ml, flash-frozen in liquid nitrogen and stored at −80°C.

In vitro pull-down assay

Purified CBC (2.9 μM) or FLAG-SRP54-NG (2.4 μM) was mixed with α-FLAG M1 agarose resin (MilliporeSigma) in the presence or absence of 5 mM $MgCl_2$ and/or 4 mM GMP-PNP (MilliporeSigma) in binding buffer consisting of buffer B and 5 mM $CaCl_2$. After 10 min of incubation with rotation at 4°C, each mixture was centrifuged, and unbound fractions collected separately. The protein-bound resin was washed three times with binding buffer only or binding buffer containing 5 mM $MgCl_2$ or 4 mM GMP-PNP. The unbound fractions and the resin-bound proteins from each experiment were loaded onto a gel for SDS-PAGE.

In vitro reconstitution assay

To prepare FLAG-tagged proteins, HEK293T cells were transiently transfected with a plasmid expressing either FLAG-GFP or IMPβ-FLAG. Two days later, IP assays were conducted using FLAG M2 affinity gels (MilliporeSigma). The bead-bound FLAG-tagged proteins were eluted with a 3×FLAG peptide (MilliporeSigma).

To prepare IMPα–CBC-associated mRNPs, HEK293T cells expressing a reporter mRNA were depleted of SRβ. The cell extracts were subjected to RNA-IP at 4°C for 3 h with either rIgG or α-CBP80 antibody pre-conjugated to protein A agarose 4B beads (Incospharm). After incubation, the beads were washed five times with NET2 buffer [50 mM Tris–HCl (pH 7.4), 150 mM NaCl, 1 mM PMSF, 2 mM benzamidine and 0.05% NP-40] supplemented with 100 U/ml RNase inhibitor (Thermo Fisher Scientific). The bead-bound RNPs were resuspended in NET2 buffer and mixed with the eluted FLAG-tagged proteins (either FLAG-GFP or IMPβ-FLAG) for 20 min at 37°C. The bead-bound and unbound fractions were then separated through centrifugation. Before RNA purification, *in vitro*-transcribed FLuc RNA molecules were added as a spike-in to both fractions.

Far-western blotting

This procedure was carried out using either purified recombinant proteins and immunopurified FLAG-SRP54-FL or its variant. Briefly, purified recombinant proteins were resolved using SDS-PAGE and transferred to a Hybond ECL nitrocellulose membrane (GE Healthcare). Each membrane was incubated in blocking buffer [100 mM Tris–HCl (pH 7.5), 100 mM potassium acetate, 2 mM magnesium acetate, 0.1 mM EDTA (pH 8.0), 10% glycerol, 1 mM PMSF, 1 mM benzamidine and 0.05% Tween 20] supplemented with 5% skimmed milk at 4°C for 24 h. The membranes were then incubated in blocking buffer containing immunopurified FLAG-SRP54-FL or its variants at 4°C for an additional 24 h. Finally, the membranes were analyzed by western blotting using HRP-conjugated α-FLAG antibody.

Immunostaining

HeLa cells, either undepleted or depleted of both SRα and CBP80, were transfected with various plasmids. Two days after plasmid transfection, the cells were fixed with 3.65–3.8% formaldehyde (MilliporeSigma) for 30 min. The fixed cells were permeabilized with 0.5% Triton X-100 (MilliporeSigma) for 10 min and then blocked with 1.5% bovine serum albumin (BSA; Bovogen, BSAS 0.1). The permeabilized cells were incubated first with a primary antibody in PBS containing 0.5% BSA and then with a rhodamine-conjugated goat α-rabbit IgG secondary antibody (31670, Thermo Fisher Scientific) and Alexa Fluor 488-conjugated goat α-mouse IgG secondary antibody (A-11017, Invitrogen).

Mitochondria were stained by incubating cells in a pre-warmed medium containing 500 nM MitoTracker (Thermo Fisher Scientific) for 30 min at 37°C. The cells were then washed with ice-cold PBS and fixed as described above. Imaging was performed using an LSM 700 or LSM 800 Carl Zeiss microscope. The images were processed using the ZEN software (Zeiss). Fluorescence intensities of the images were quantitated using ImageJ.

In situ proximity ligation assay (PLA)

This assay was performed using the *in situ* Proximity Ligation Assay Kit (MilliporeSigma), following the manufacturer's instructions. Briefly, the cells were fixed with formaldehyde and permeabilized with 0.5% Triton X-100 in PBS. The permeabilized cells were incubated in blocking buffer at 37°C for 1 h and then probed with primary antibodies in antibody diluent buffer at 37°C for 1 h. After washing, the cells were incubated for 1 h with secondary antibodies conjugated with either a PLUS or MINUS PLA probe [Duolink® In Situ PLA® Probe Anti-Mouse PLUS (MilliporeSigma; DUO82001) and Duolink® In Situ PLA® Probe Anti-Rabbit MINUS (MilliporeSigma; DUO82005)] at 37°C. The PLA probes were ligated in ligation buffer at 37°C for 30 min and amplified in a polymerase mixture with rolling circle amplification Green buffer at 37°C for 100 min. Finally, the cells were stained with DAPI and imaged using an LSM 800 confocal microscope (Carl Zeiss). To quantify the PLA signal in Figure 6C, over

50 cells were counted from three biological replicates, and the number of PLA puncta was counted using ImageJ. *P* values were computed using Wilcoxon's signed-rank test.

Determination of intracellular ADP/ATP ratio

This ratio was measured in HEK293T cells (1×10^3) using the ADP/ATP Ratio Assay Kit (MilliporeSigma) according to the manufacturer's instructions. Briefly, cells were incubated in ATP reagent for 1 min, and luminescence was quantified as a metric of the amount (A) of ATP. After incubation for an additional 10 min, background luminescence was quantified again prior to ADP measurement (B). ADP was quantified by adding an ADP-converting enzyme (C). The ADP/ATP ratio was calculated as follows: ADP/ATP ratio $= (C - B)/A$.

Measurement of mitochondrial membrane potential

Mitochondrial membrane potential was measured in HEK293T cells using the TMRE Mitochondrial Membrane Potential Assay Kit (BioVision), according to the manufacturer's instructions. Cells (1×10^4) were cultured in a 96-well plate. Three days after siRNA transfection, the cells were incubated with 200 nM TMRE at 37°C for 30 min in the dark. After that, the cells were washed three times with 100 μl assay buffer. Fluorescent signals were measured at excitation/emission wavelengths of 549/575 nm using a fluorescence microplate reader (Bio-Rad).

Generation of cell lines

HEK293FT cells stably expressing Myc-eIF4E were generated by cotransfection with a plasmid expressing Myc-eIF4E and a plasmid expressing a puromycin resistance gene. Two days after transfection, the cells were serially diluted and maintained in DMEM supplemented with 1 μg/ml puromycin (MilliporeSigma) until distinct colonies formed. Independent colonies were isolated and subjected to western blotting with either α-eIF4E or α-Myc antibodies to determine the relative expression level of Myc-eIF4E compared to endogenous eIF4E. The selected cell lines were maintained in DMEM supplemented with 0.5 μg/ml puromycin.

Polysome fractionation experiments

HEK293FT cells cultured in two 150 mm culture dishes were harvested. The cytoplasmic extracts were assayed using polysome fractionation experiments, as described elsewhere (29,37). Each pooled fraction was then subjected to IP with various antibodies.

Where indicated, HEK293FT cells stably expressing Myc-eIF4E were transfected with the indicated siRNAs. One day after transfection, the cells were re-transfected with various plasmids and two days later, polysomal fractionation experiments were conducted as described above.

DNA microarray analysis

This analysis was performed at eBiogen (Republic of Korea). HEK293FT cells were subjected to polysome fractionation experiments and the polysomal fractions were pooled for RNA-IP using either α-CBP80 or α-eIF4E antibodies. Bound RNA was purified and converted to Cy3/5-labeled complementary RNA (cRNA) using the Low RNA Input Linear Amplification Kit (Agilent Technologies). The Cy3/5-labeled cRNA was then hybridized onto Agilent's Human Oligo Microarray (44 K human gene chip). Hybridization images were captured using Agilent's DNA microarray scanner and quantified using the Feature Extraction Software (Agilent Technologies). Data normalization and selection of differentially expressed genes were performed using GeneSpring GX 7.3 (Agilent Technologies). The averages of normalized ratios were calculated by dividing the average of normalized signal channel intensities by the average of the normalized control channel intensities.

QuantSeq 3′ mRNA sequencing

Co-immunoprecipitated (Co-IPed) transcripts were extracted from CBP80 or SRP68 immunoprecipitates using TRIzol Reagent. RNA quality was analyzed on an Agilent 2100 Bioanalyzer using the RNA 6000 Nano Chip (Agilent Technologies). RNA quantity was measured using an ND-2000 spectrophotometer (Thermo Scientific). RNA libraries were constructed using the QuantSeq 3′ mRNA Seq Library Prep Kit (Lexogen) and then subjected to high-throughput sequencing as single-end (1×75 bp) reads on NextSeq 500 (Illumina) at eBiogen Inc.

Poly(A)$^+$ high-throughput RNA sequencing (RNA-seq)

Poly(A)$^+$ RNA-seq libraries were constructed and sequenced at Macrogen Inc. Poly(A)$^+$ RNA was purified using oligo-d(T)-conjugated magnetic beads. The libraries were prepared using TruSeq Stranded mRNA Sample Prep Kit (Illumina). The quality of the final libraries was tested on an Agilent Bioanalyzer (DNA 1000 kit; Agilent Technologies). They were then quantified using qPCR (Kapa Library Quant Kit; Kapa Biosystems, Wilmington, MA). Libraries were sequenced in paired-end mode (2×100 bp) on an Illumina HiSeq 2500 (Illumina, CA, USA).

Next-generation sequence data analysis

Reads obtained from QuantSeq were mapped to the human reference genome (hg19) using Bowtie2 (38). Bowtie2 indexes were generated either from the genome assembly sequence or from representative transcript sequences. Differentially expressed genes were analyzed in Bedtools based on read counts obtained from the alignment coverage (39).

To analyze Poly(A)$^+$ RNA-seq data, adaptor sequences were first trimmed from the reads using Cutadapt (40). Reads over 15 bp long and with Phred quality scores higher than 30 were selected. The processed reads were aligned to the reference human genome (hg19) using STAR aligner software (41). Read counts per gene were estimated using the htseq-count Python code (42). Each RPM value was used to normalize co-IPed RNA. The normalized values (RPM of co-IPed RNA/RPM of input RNA) were filtered based on a 1.0 cutoff. The filtered genes were classified into two groups: 'CBP80-bound mRNAs' and 'SRP68-bound mRNAs' (Figure 2D). CBP80-bound mRNAs in cells depleted of SRα and SRβ were processed in the same way.

CBP80-bound mRNAs were categorized into three groups: CBP80 IP (present in the CBP80 IP), CBP80 IP–SRP68 IP (present only in the CBP80 IP but not in the SRP68 IP), and CBP80 IP ∩ SRP68 IP (present in both CBP80 IP and SRP68 IP and therefore able to form the CBC–RNC–SRP complex). The $\log_2$ (si*SRα/β* ÷ siControl) value of each group was presented as a CDF plot.

Gene ontology (GO) analysis

A target group (fold change ≥ 1.5) was uploaded to DAVID (43,44) and analyzed using the functional annotation tool. GO terms from the cellular component category were used in this study. The results file was retrieved, and the GO terms and their corresponding P values were retrieved.

Statistical analysis

Two-tailed equal-variance Student's *t* test was performed, with significance defined as a *P* value <0.05 or <0.01. Data are presented as the mean ± standard deviation.

For CDF analysis, *P* values were calculated using the two-tailed Mann–Whitney *U* test. Pearson's correlation coefficients (*r*) were calculated to determine correlation between mRNA sequence data and QuantSeq data obtained from two biological replicates.

P values associated with the quantification of PLA puncta (Figure 6C) were computed using Wilcoxon's signed-rank test.

RESULTS

The CBC physically interacts with the SRP

We were curious about a possible difference in composition between CBC-associated mRNAs and eIF4E-associated mRNAs during their translation. To this end, pooled polysomal fractions were separated into two fractions by immunoprecipitation (IP) using either an anti- (α-) CBP80 or an α-eIF4E antibody (Supplementary Figure S1A). Microarray analysis of coimmunoprecipitated (co-IPed) transcripts revealed that although most cellular mRNAs and ncRNAs were associated with CBP80 and eIF4E in comparable ratios, subsets of mRNAs and ncRNAs were preferentially enriched in the IPs of CBP80 (Figure 1A, Supplementary Figure S1B, and Supplementary Table S2). One of the top-ranked ncRNAs was RN7SL1, an ncRNA component of the SRP complex (Figure 1A, Supplementary Figure S1C, and Supplementary Table S2B). The specific interaction between CBP80 and the SRP was evidenced using different approaches: IPs (Supplementary Figures S2 and S3A–D), far-western blotting (Figure 1B), and *in vitro* pull-down assay using purified recombinant proteins (Figure 1C). Furthermore, on the basis of publicly available structural data on human SRP54 and SRα (PDB: 5L3Q) (45) and CBP80–CBP20–PGC1β complex (PDB: 6D0Y) (46), we predicted three possible residues critical for the interaction between CBP80 and SRP54: L34, L254 and L264, present at the N-terminal domain of CBP80 (residues 1–307), since hydrophobic residues usually play a major role in protein–protein interactions. These residues are located on the protein surface and are expected to have minimal effect on protein folding. Among these, the L34E substitution in CBP80 specifically disrupted its association with SRP54 (Figure 1D and Supplementary Figure S3E). These data indicate that the CBC directly interacts with the SRP through the N-terminal MIF4G domain of CBP80 and the NG domain of SRP54 (Figure 1E).

It is known that the NG domain of SRP54 directly interacts with the NG domain of SRα on the ER surface, allowing the RNC–SRP complex to dock to the ER (47,48). Based on our observations, we hypothesized that CBP80 may compete with SRα for binding to SRP54 (Figure 1E). In support of this hypothesis, SR downregulation increased the association between CBP80 and SRP without affecting the interaction between CBP80 and IMPα (Figure 1F and Supplementary Figure S4A). Furthermore, overexpression of the NG domain, but not the SRX domain, of SRα disrupted the association between CBP80 and SRP54 (Supplementary Figure S4B).

Inefficient targeting of RNC–SRP to the ER results in accumulation of the CBC–RNC–SRP complex

We investigated changes in mRNP composition due to the observed competition by employing a *Renilla* luciferase (RLuc) reporter mRNA (Figure 2A) either lacking (Con-RβGl) or harboring (PPL-RβGl) an ER-targeting signal sequence (which interacts with the SRP) derived from a secretory protein, preprolactin (hereafter referred to as PPL) (19). CBC-associated and eIF4E-associated reporter mRNPs were separated through IP, using either α-CBP80 antibody or α-eIF4E antibody. Although the amount of CBP80-associated Con-RβGl mRNA was affected only marginally by SR downregulation, the amount of CBP80-associated PPL-RβGl mRNA was significantly increased by this downregulation (Figure 2B and Supplementary Figure S5A). In contrast, no increase was observed for eIF4E-associated Con-RβGl or PPL-RβGl mRNA (Figure 2B and Supplementary Figure S5B). Notably, an increase in the amount of CBP80-associated PPL-RβGl mRNA was only observed in the IP of CBP80-WT, but not of CBP80-L34E (Supplementary Figure S5C and D). These results provide evidence that inefficient binding of RNC–SRP to the SR (caused by SR downregulation) results in specific accumulation of mRNP (destined for ER) in the form of the CBC–RNC–SRP complex (Figure 2C).

The specific accumulation was validated at the transcriptome level (Figure 2D, E, and Supplementary Figure S6A–D). We identified 2,778 mRNAs commonly enriched in two biological replicates of the IP of CBP80 and 1922 mRNAs commonly enriched in two biological replicates of the IP of SRP68 (another component of the SRP) (Figure 2D and Supplementary Table S3). The obtained mRNAs were categorized into three groups: CBP80 IP group (present in the CBP80 IP), CBP80 IP – SRP68 IP group (present only in the CBP80 IP but not in the SRP68 IP), and CBP80 IP ∩ SRP68 IP group (present in both CBP80 IP and SRP68 IP and therefore able to form the CBC–RNC–SRP complex). Based on cumulative distribution function (CDF) analysis, the CBP80 IP ∩ SRP68 IP group showed a significant increase in fold enrichment in the IP of CBP80 following SR downregulation compared with the other groups (Figure 2E). These transcriptome data showed that mRNAs associated with both CBP80 and SRP68 were preferentially en-

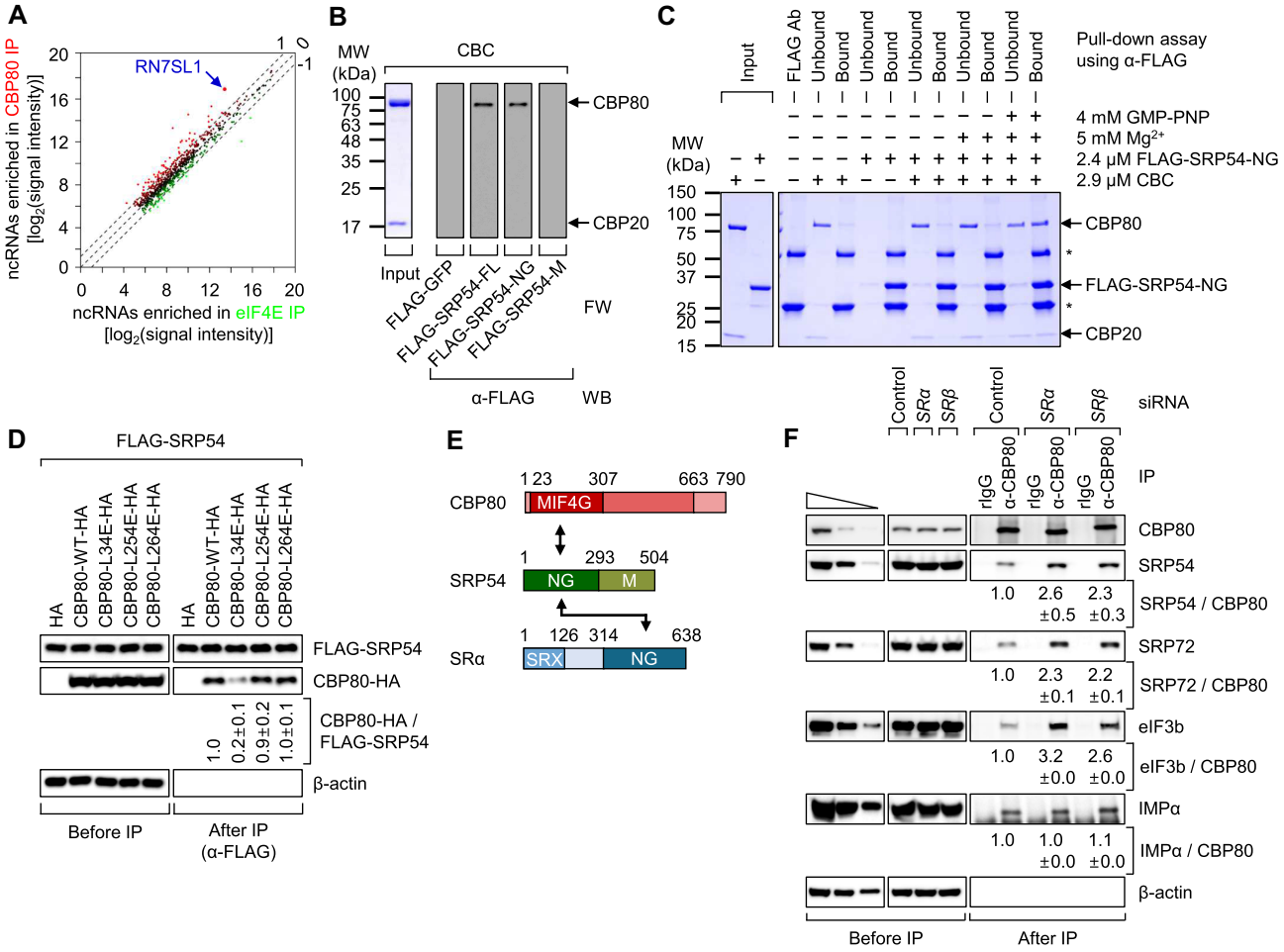

Figure 1. The CBC directly interacts with the SRP. (**A**) The scatter plot of ncRNAs enriched in the IP of CBP80 and eIF4E ($\log_2$ scale). Co-IPed ncRNAs obtained from two independently conducted polysome fractionation experiments followed by IP were studied by microarray analysis. (**B**) Far-western blotting (FW) of purified recombinant proteins. (left) Coomassie blue staining of a purified recombinant CBC. (right) FW of immunopurified FLAG-SRP54—either full-length (FL) or its deletion variant—as a probe; $n = 2$. (**C**) *In vitro* pull-down assays of purified recombinant proteins (the CBC and FLAG-SRP54-NG) using α-FLAG antibody. After pull-down, samples of bead-bound or unbound proteins were stained with Coomassie blue. GMP-PNP, a nonhydrolyzable analog of GTP; *, heavy and light chains of IgG; $n = 2$. (**D**) IP of SRP54. IP with α-FLAG antibody was carried out using extracts of HEK293T cells transiently expressing FLAG-SRP54 and either CBP80-WT-HA or its variant. Levels of co-IPed CBP80-HA were normalized to those of IPed FLAG-SRP54; $n = 3$. (**E**) Schematic representation of the domains in CBP80, SRP54, and SRα. The arrows indicate domain interactions observed in this or previous studies. MIF4G domain, the middle domain of eIF4G; NG domain, the helical N-domain and the central GTPase domain; M domain, methionine-rich domain; SRX, SRβ-interacting domain. (**F**) IP of endogenous CBP80. IP was carried out using either α-CBP80 antibody or, as a control, rabbit IgG (rIgG), in the extracts of HEK293T cells either undepleted or depleted of either SRα or SRβ; $n = 2$.

riched in the IP of CBP80 upon SR downregulation, suggesting that inefficient binding of RNC–SRP to the SR leads to preferential accumulation of the CBC–RNC–SRP complex. This conclusion was further supported by evidence showing preferential enrichment of endogenous mRNAs belonging to the CBP80 IP ∩ SRP68 IP group in the IP of CBP80-WT, but not CBP80-L34E, upon SR downregulation (Supplementary Figure S6E).

The CBC–RNC–SRP complex is resistant to IMPβ-mediated mRNP remodeling

How does the inefficient binding of RNC–SRP to the SR lead to accumulation of the CBC–RNC–SRP complex? We noted that fewer CBP80 and IMPα were enriched in the IP of IMPβ following SR downregulation (Supplementary Figure S7A and B), implying that the CBC–RNC–SRP complex may not be favorable for IMPβ-mediated mRNP remodeling (25,26).

To test this hypothesis, we conducted an *in vitro* reconstitution assay (Figure 3 and Supplementary Figure S7C–F). Either CBC-associated Con-RβGl or PPL-RβGl mRNP was immunopurified by IP using α-CBP80 antibody and extracts of cells either undepleted or depleted of SRβ (Figure 3A, right). In parallel, either transiently expressed IMPβ-FLAG or FLAG-GFP (used as a control) was immunopurified and eluted from the beads (Figure 3A, left). The eluted protein (IMPβ-FLAG or FLAG-GFP) was mixed with CBC-associated mRNPs bound to agarose beads. For CBC-associated Con-RβGl mRNPs, the addition of IMPβ-FLAG resulted in a ∼2-fold reduction in the amount of bead-bound reporter mRNAs immunopurified from either

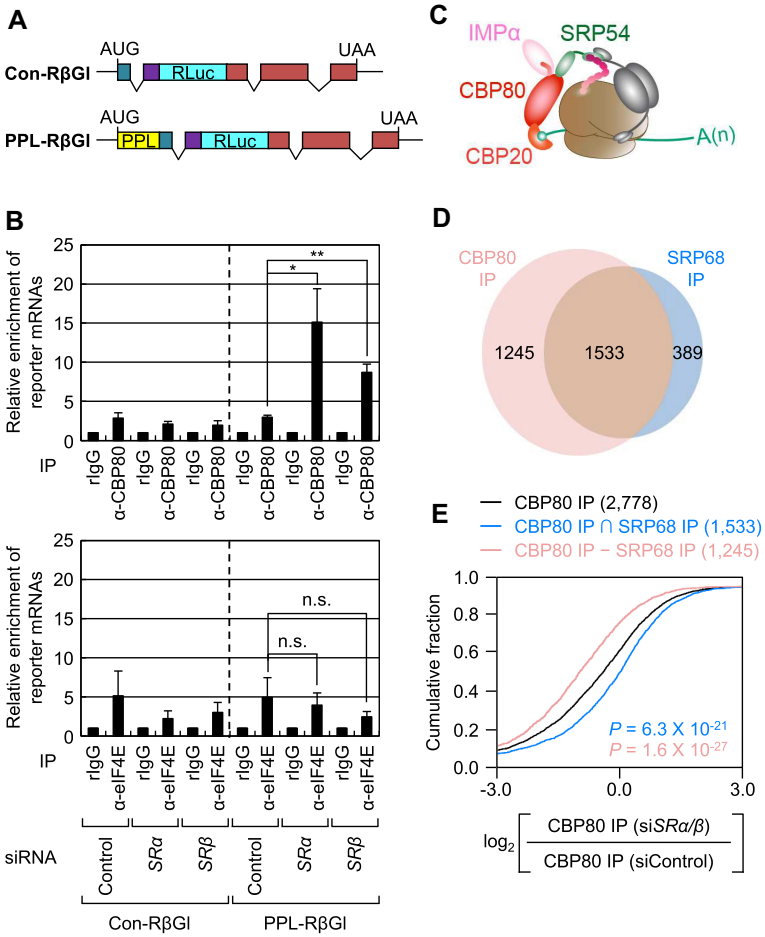

Figure 2. Downregulation of the SR results in accumulation of the CBC–RNC–SRP complex. (**A**) A schematic of reporter mRNAs. PPL, a signal sequence derived from preprolactin. (**B**) Relative abundance of co-IPed reporter mRNAs in the IPs of either CBP80 (upper) or eIF4E (lower) following downregulation of either SRα or SRβ in HEK293T cells. After the IPs, *in vitro*–transcribed firefly luciferase (FLuc) RNAs were added to each IP as a spike-in. The levels of co-IPed reporter mRNAs were normalized to that of FLuc RNA; $n = 4$. *$P < 0.05$; **$P < 0.01$; n.s., not significant. (**C**) A schematic of the CBC–RNC–SRP complex assembled on an mRNA encoding a signal sequence. (**D**) Venn diagrams showing the number of mRNAs enriched in the IP of CBP80 or SRP68. Only mRNAs with reads per million (RPM) values over 1.0 were selected for further analysis. (**E**) A CDF plot showing relative changes in the abundance of co-IPed mRNAs in CBP80 after SR downregulation. The *P* value was calculated using two-tailed Mann–Whitney *U* test.

undepleted or SRβ-depleted cells (Figure 3B), confirming the efficient dissociation of mRNA from the CBC–mRNP complex under our experimental conditions. In contrast, in the case of CBC-associated PPL-RβGl mRNPs, the addition of IMPβ-FLAG reduced the amount of bead-bound reporter mRNAs immunopurified from undepleted cells, but not from SRβ-depleted cells (Figure 3C). These results suggest that the CBC–RNC–SRP complex is resistant to IMPβ-mediated replacement of the CBC by eIF4E and thus accumulates when RNC–SRP fails to interact with the SR on the surface of the ER.

The CBC–RNC–SRP complex is translationally repressed

Next, we investigated the translational competence of the accumulated CBC–RNC–SRP complex (Figure 4). Cytoplasmic extracts were prepared from either undepleted or SRβ-depleted HEK293FT cells expressing Myc-eIF4E, CBP80-HA, and reporter mRNAs (both Con-RβGl and PPL-RβGl mRNAs) (Figure 4A). Subsequently, each fraction obtained from the polysome fractionation experiments was subjected to IP using either α-HA antibody (for isolation of CBC-associated mRNPs) or α-Myc antibody (for isolation of eIF4E-associated mRNPs) (Figure 4B).

The relative distribution of CBP80-associated PPL-RβGl mRNAs, but not eIF4E-associated PPL-RβGl mRNAs, drastically shifted from polysomal to subpolysomal fractions after SRβ downregulation (Figure 4C and D). In contrast, the relative distribution of either CBP80- or eIF4E-associated Con-RβGl mRNAs was not significantly affected by SRβ downregulation (Figure 4E and F), suggesting that CBC–RNC–SRP is a translationally repressed complex. Remarkably, double downregulation of both CBP80 and SRβ promoted preferential enrichment of eIF4E-associated PPL-RβGl mRNAs, but not eIF4E-associated Con-RβGl mRNAs, in the polysomal fractions (Supplementary Figure S8), implying that a failure of the interaction between the CBC and SRP causes an IMPβ-mediated replacement of the CBC by eIF4E, consequently promoting the translation of the resulting eIF4E–RNC–SRP. These data indicate that inefficient targeting of RNC–SRP to the ER renders RNC–SRP translationally repressed

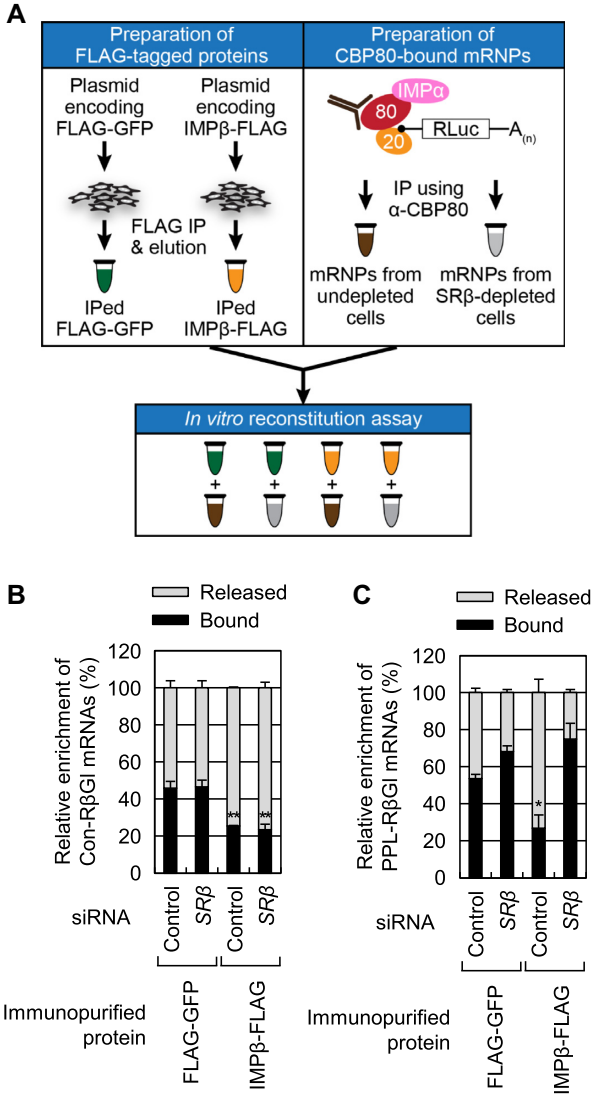

Figure 3. The CBC–RNC–SRP complex is resistant to IMPβ-mediated mRNP remodeling. *In vitro* reconstitution assays were performed using immunopurified proteins and IMPα–CBC-associated mRNPs. (**A**) Schematic of the experimental scheme for the *in vitro* reconstitution assay. To prepare FLAG-GFP or IMPβ-FLAG, the IPs with α-FLAG antibody–conjugated agarose beads were carried out in extracts of HEK293T cells transiently expressing either FLAG-GFP or IMPβ-FLAG. Bead-bound FLAG-GFP or IMPβ-FLAG was eluted using the FLAG peptide. To prepare IMPα–CBP80-associated mRNPs, the IPs using either α-CBP80 antibody or rIgG were performed in extracts of HEK293T cells transiently expressing a reporter mRNA (either Con-RβGl or PPL-RβGl) and either undepleted or depleted of SRβ. After incubating the eluted proteins and the bead-bound IMPα–CBP80-bound mRNPs, *in vitro*-transcribed *FLuc* RNAs were added as a spike-in to the obtained bead-bound or released fractions. The relative amounts of either bead-bound or released mRNAs were quantified using quantitative reverse-transcription PCR (qRT-PCR), and the results were normalized to *FLuc* RNAs. (**B**) *In vitro* reconstitution assay of IMPα–CBP80-bound Con-RβGl reporter mRNAs. $n = 3$; $^{**}P < 0.01$. (**C**) *In vitro* reconstitution assay using IMPα–CBP80-bound PPL-RβGl reporter mRNAs. $n = 3$; $^{*}P < 0.05$.

through the CBP80–SRP54 interaction. This CBC-ensured translational repression of RNC–SRP until its proper targeting to the ER is hereafter referred to as 'CENTRE.'

Our concept of CENTRE was corroborated through experiments using glutathione peroxidase 1 (*GPx1*) reporter mRNAs; either Con-FLAG-GPx1 mRNA or PPL-FLAG-GPx1 mRNA (Supplementary Figure S9A). Downregulation of SRα resulted in a ∼5-fold reduction in the expression of polypeptides from PPL-FLAG-GPx1 mRNA, but not from Con-FLAG-GPx1 mRNA. However, this was reversed by the double downregulation of SRα and CBP80 without significantly affecting the abundance of reporter mRNAs (Figure 5A and Supplementary Figure S9B). A similar expression pattern was observed for Myc-ER-GFP reporter mRNA encoding a signal sequence (Figure 5B and Supplementary Figure S9C) and DPM3-GFP reporter mRNA (Supplementary Figure S9D and E). *DPM3* mRNA belonged to the CBP80 IP ∩ SRP68 IP group and showed a ∼4.9-fold increase in the IP of CBP80 following SR downregulation (Figure 2D, E, and Supplementary Table S3B). Treating the cells with MG132, a potent proteasome inhibitor, did not affect the amount of expressed polypeptides, ruling out an indirect effect on protein stability.

We also carried out a complementation assay using either small interfering RNA (siRNA)-resistant CBP80^{R}-wild type (WT) or CBP80^{R}-L34E and siRNAs against SRα and CBP80. When cells were depleted of both SRα and CBP80, expression of CBP80^{R}-WT, but not CBP80^{R}-L34E, reduced the expression of polypeptides from PPL-FLAG-GPx1 mRNA (Figure 5C) and Myc-ER-GFP reporter mRNA (Figure 5D) by ∼13-fold and ∼4-fold, respectively, marginally affecting the abundance of reporter mRNAs (Supplementary Figure S9F and G). These findings suggest that mRNAs encoding a signal sequence are subjected to CENTRE, and that in the event that CENTRE is inefficient, CBC–RNC–SRP is easily converted to eIF4E–RNC–SRP with the help of IMPβ, and the resulting eIF4E–RNC–SRP can be promiscuously translated even before proper targeting of RNC–SRP to the ER.

CENTRE safeguards against accumulation of protein aggregates in the cytosol

What is the biological importance of CENTRE? Under normal conditions, the intracellular distribution of Myc-ER-GFP or DPM3-GFP largely overlapped with that of a well-characterized ER-resident protein, Sec61β (Figure 6A and Supplementary Figure S10), which is translocated to the ER in an SRP-independent manner (49,50). In contrast, double downregulation of SRα and CBP80 caused aberrant localization of Myc-ER-GFP or DPM3-GFP to peculiar cytoplasmic aggregates that did not overlap with Sec61β (Figure 6A, Supplementary Figures S10 and S11A). The observed protein aggregates partially overlapped with ubiquitin (Supplementary Figure S11B) but not with non-membranous cytosolic aggregates (aggresomes, processing bodies, and stress granules), autophagy puncta, and membranous organelles (mitochondria and lysosomes; Supplementary Figure S11C–H). Of note, complementation with

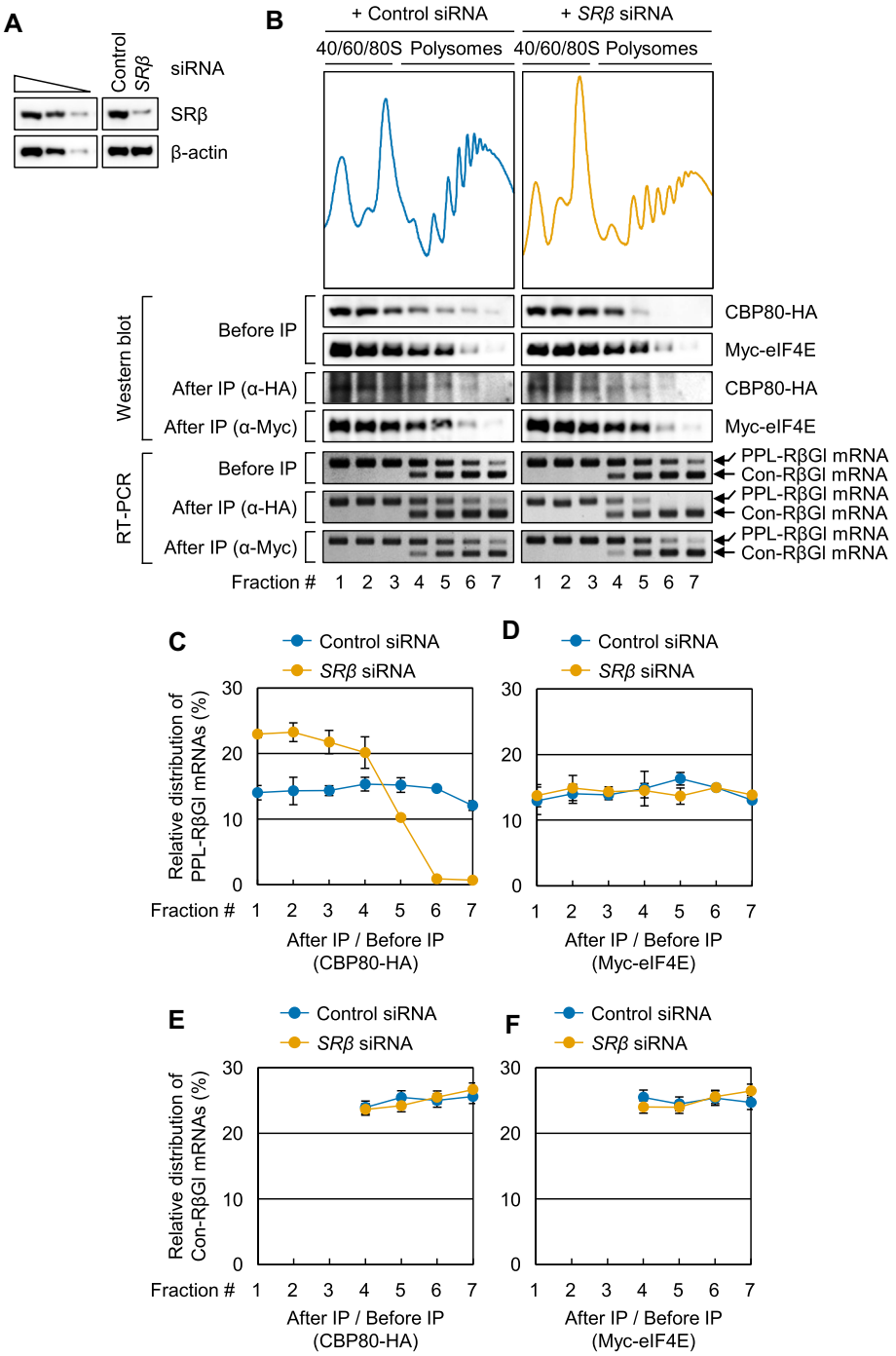

Figure 4. The CBC–RNC–SRP complex accumulates subpolysomal fractions following SRβ downregulation. HEK293FT cells stably expressing Myc-eIF4E were either undepleted or depleted of SRβ, and then were transiently expressed with CBP80-HA and two reporter mRNAs (Con-RβGl and PPL-RβGl mRNAs). The cytoplasmic extracts were then subjected to polysome fractionation experiments followed by IP with either α-HA or α-Myc antibody. (**A**) Western blotting assay confirming specific downregulation of SRβ. (**B**) Relative distribution of IPed proteins and co-IPed reporter mRNAs in polysome-fractionated samples. (**C** and **D**) Relative distribution of PPL-RβGl mRNAs. Amounts of PPL-RβGl mRNAs after the IPs were normalized to those before IPs. Relative distribution of normalized PPL-RβGl mRNAs co-immunopurified with either CBP80-HA (panel C) or Myc-eIF4E (panel D) are presented as a percentage of normalized ratios; n = 2. (**E** and **F**) Relative distribution of Con-RβGl mRNAs. As performed in (C), (D), except that the relative distribution of normalized Con-RβGl mRNAs co-immunopurified with CBP80-HA (panel E) or Myc-eIF4E (panel F) are presented as a percentage of the normalized ratios; $n = 2$.

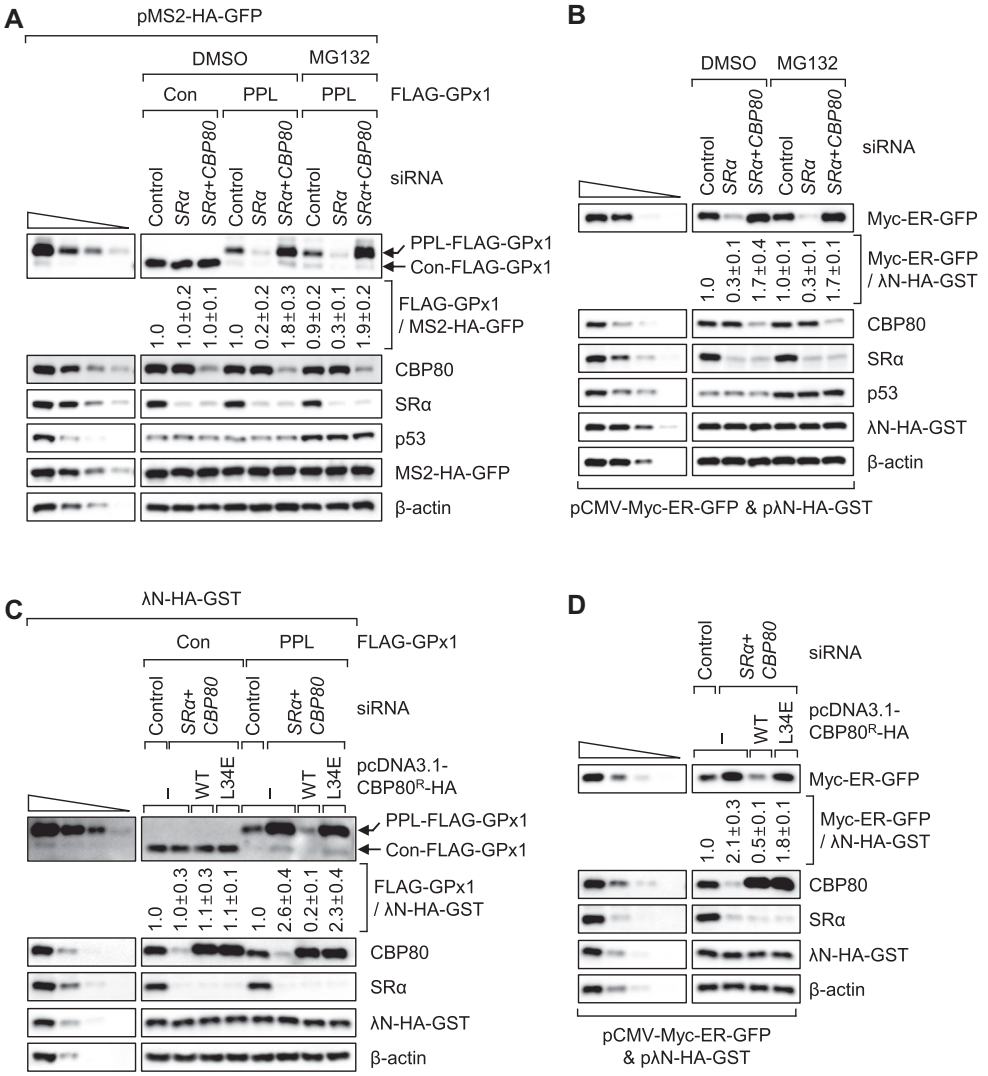

Figure 5. The CBC–RNC–SRP complex is translationally repressed. (**A**) Protein expression from Con-FLAG-GPx1 or PPL-FLAG-GPx1 mRNA. HEK293T cells depleted of the indicated protein were transiently transfected with one of reporter plasmids and pMS2-HA-GFP (a reference plasmid). The cells were either untreated or treated with MG132 for 12 h before cell harvesting. The levels of the expressed proteins were normalized to MS2-HA-GFP protein abundance. Efficient inhibition of proteasomal activity by MG132 treatment was evidenced by an increase in the abundance of endogenous p53 through its stabilization; $n = 3$. (**B**) Protein expression from Myc-ER-GFP mRNAs. As performed in panel A, except that HEK293T cells were transiently transfected with pCMV-Myc-ER-GFP and a reference plasmid expressing λN-HA-GST; $n = 3$. (**C**) Complementation experiments using CBP80^{R}-WT or -L34E variant and either Con-FLAG-GPx1 mRNA or PPL-FLAG-GPx1 mRNA. As performed in panel A, except that HEK293T cells, either undepleted or depleted of both SRα and CBP80 were transiently transfected with (i) a plasmid expressing either CBP80^{R}-WT-HA or CBP80^{R}-L34E-HA, (ii) a reporter plasmid expressing Con-FLAG-GPx1 or PPL-FLAG-GPx1 mRNA, and (iii) a reference plasmid, λN-HA-GST; $n = 3$. (**D**) Complementation experiments using CBP80^{R}-WT or -L34E and Myc-ER-GFP mRNAs. As performed in panel C, except that protein expression from Myc-ER-GFP mRNA was analyzed; $n = 3$.

siRNA-resistant CBP80^{R}-WT, but not CBP80^{R}-L34E, restored the colocalization of either Myc-ER-GFP or DPM3-GFP with Sec61β (Figure 6A and Supplementary Figure S10). In addition, a proximity ligation assay (PLA) showed that SRα downregulation increased PLA signals of CBP80 and SRP54 in the cytosol (Figure 6B and C), pointing to selective accumulation of the CBC–RNC–SRP complex in the cytosol. In contrast, PLA signals of eIF4E and SRP54 were not detectable in cells that were undepleted, depleted of SRα alone, or depleted of both SRα and CBP80 (Figure 6D). Altogether, these results suggest that a failure of CENTRE causes promiscuous synthesis of signal sequence-containing polypeptides from RNC–SRP before its targeting to the ER, resulting in accumulation of aberrant polypeptides in the cytosol.

CENTRE mitigates a cytosolic stress response

When misfolded protein aggregates accumulate in the cytosol under stress conditions, a cytosolic stress response (CSR) typified by the heat shock response is induced to restore protein homeostasis (16). CSR activates heat shock factor 1 (HSF1) and subsequently induces the transcription of genes encoding heat shock proteins (HSPs). Therefore, we investigated the effect of cytosolic protein aggregates generated by inefficient CENTRE on CSR.

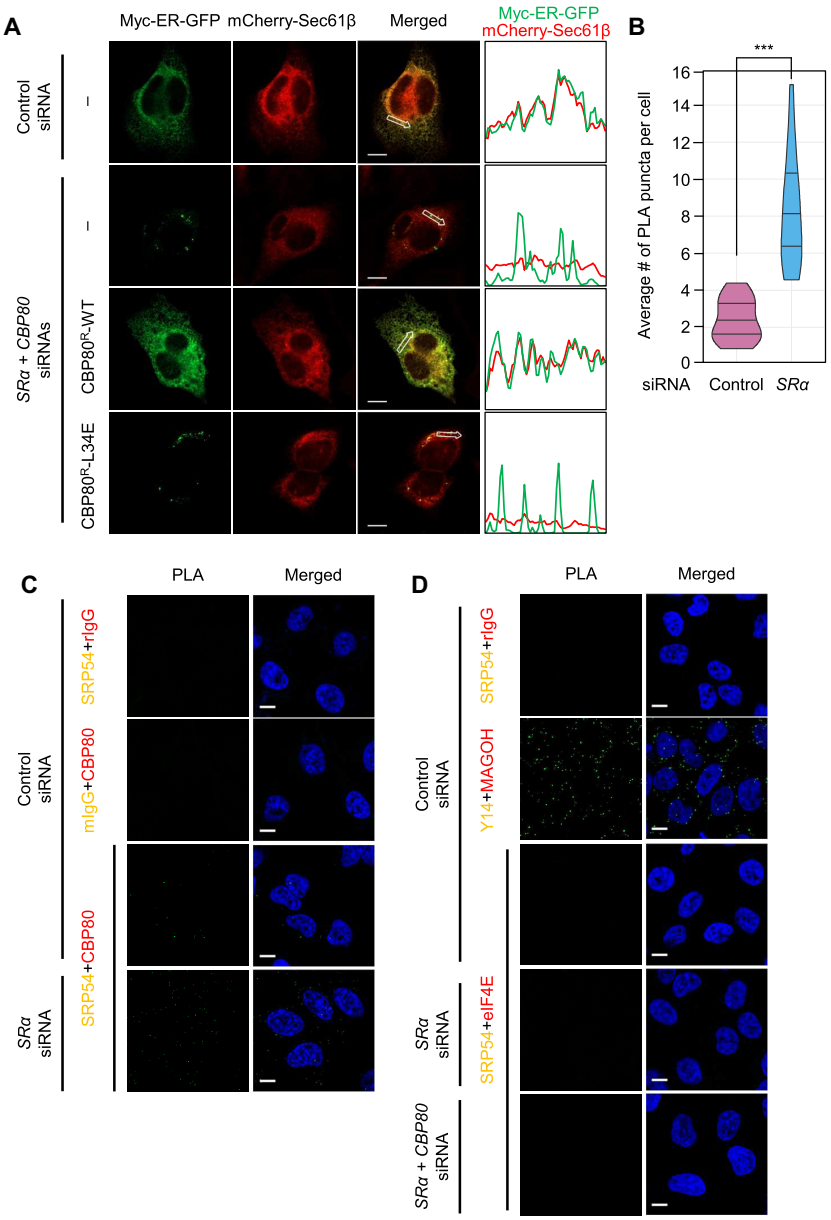

Figure 6. Inefficient CENTRE leads to accumulation of protein aggregates. (**A**) Confocal imaging of the Myc-ER-GFP protein and mCherry-Sec61β. HeLa cells depleted of the indicated proteins were transiently transfected with a plasmid expressing Myc-ER-GFP, a reference plasmid expressing mCherry-Sec61β, and HA, CBP80^{R}-WT-HA, or CBP80^{R}-L34E-HA. Scale bar, 10 μm; $n = 3$. (B and C) PLA for CBP80 and SRP54. HeLa cells, either undepleted or depleted of SRα, were subjected to PLA (**B**) Quantitation of PLA signals for endogenous CBP80 and SRP54. More than 50 cells from three biological replicates were quantitated. (**C**) PLA images. The antibodies raised in a mouse or rabbit are colored in yellow or red, respectively. mIgG, nonspecific mouse IgG; rIgG, nonspecific rabbit IgG; scale bar, 10 μm; $n = 3$. (**D**) PLA for eIF4E and SRP54. A previously known interaction between Y14 and MAGOH served as a positive control; $n = 3$; scale bar, 10 μm.

Double downregulation of SRα and CBP80 significantly promoted CSR (transcriptional induction of HSP mRNAs) and delayed the restoration time of CSR following heat shock, compared with single downregulation (Figure 7A). The observed effects were reversed by HSF1 downregulation (Figure 7B and C), suggesting that the CSR promoted by double downregulation is mediated by HSF1. In addition, the enhancement in CSR observed following double downregulation was significantly attenuated by the expression of CBP80^{R}-WT, but not of the CBP80^{R}-L34E variant (Figure 7D and E). Of note, complementation with CBP80^{R}-WT, but not with CBP80^{R}-L34E, blocked the phosphorylation induced by double downregulation at the S326 residue of HSF1 (Figure 7D), suggesting that the phosphorylation at S326, a previously characterized key residue that is phosphorylated upon HSF1 activation (51), is involved in the CSR promoted by double downregulation. These data indicate that the cytosolic protein aggregates generated by inefficient CENTRE promote CSR via HSF1.

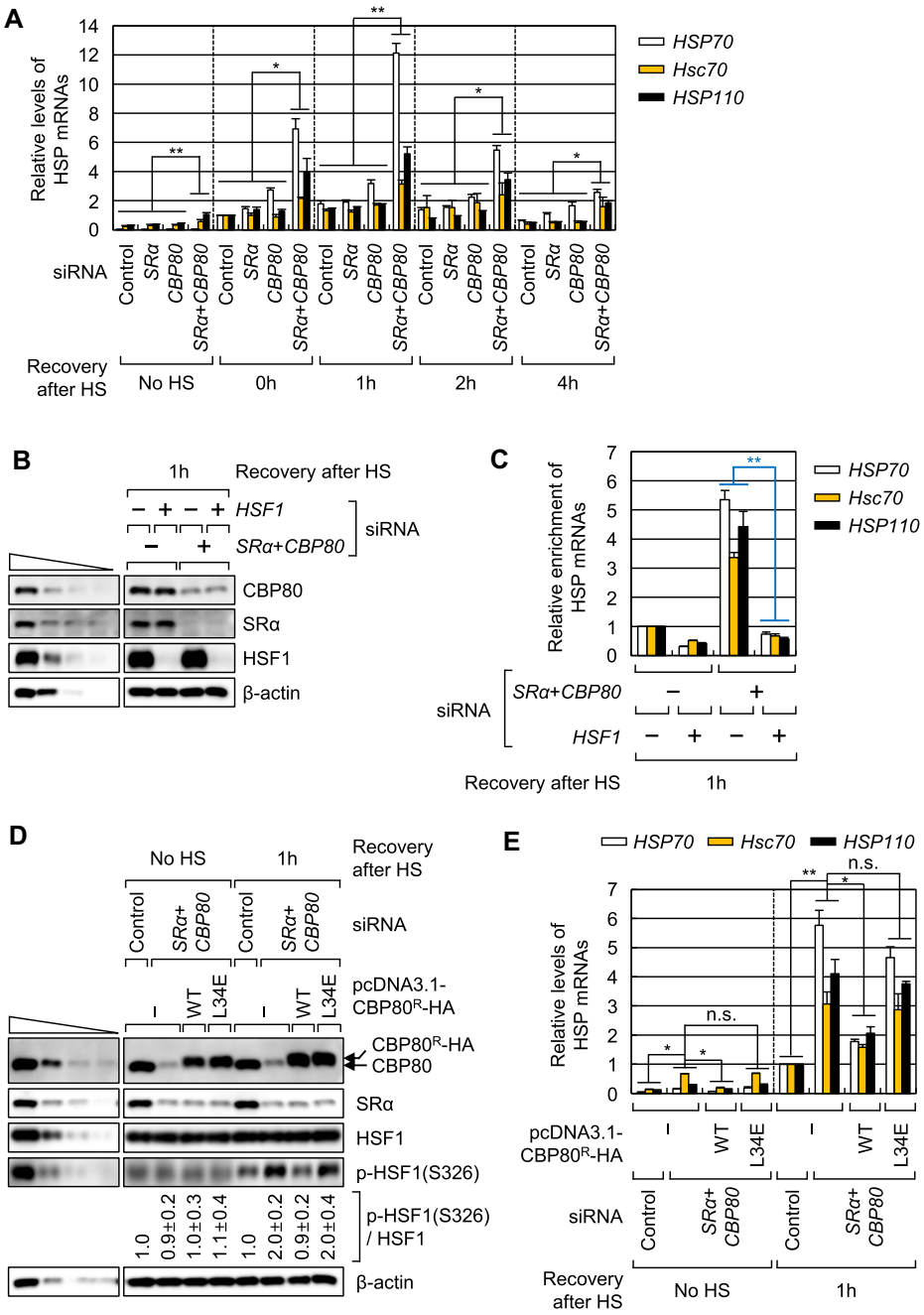

Figure 7. Inefficient CENTRE promotes a cytosolic stress response. (**A**) Effects of single downregulation (of either SRα or CBP80) or double downregulation (of both SRα and CBP80) on the CSR. HeLa cells depleted of the indicated proteins were either untreated or treated with heat shock at 42°C for 30 min and then recovered at 37°C for the indicated periods. The levels of HSP mRNAs were normalized to those of endogenous *GAPDH* mRNA. Normalized levels of HSP mRNAs in undepleted cells treated with heat shock and restored for 0 h were arbitrarily set to 1.0. HS, heat shock; $n = 3$; $^{*}P < 0.05$; $^{**}P < 0.01$. (B and C) Effects of HSF1 downregulation on the CSR induced by CENTRE failure. As performed in panel A, except that HeLa cells were either undepleted or depleted of the indicated proteins. The normalized levels of HSP mRNAs in undepleted cells treated with heat shock and restored for 1 h were arbitrarily set to 1.0. HS, heat shock; $n = 3$; $^{**}P < 0.01$. (**B**) Western blotting showing specific downregulation. (**C**) Relative levels of HSP mRNAs. (D and E) The complementation experiment. HeLa cells depleted of the indicated proteins were transiently transfected with a plasmid expressing CBP80^{R}-WT-HA or CBP80^{R}-L34E-HA. Then, the cells were either untreated or treated with heat shock at 42°C for 30 min and then recovered at 37°C for 1 h. (**D**) Western blotting confirming specific downregulation of endogenous CBP80 and comparable expression of siRNA-resistant CBP80^{R}-WT-HA or CBP80^{R}-L34E-HA. HS, heat shock; p-HSF1, phosphorylated HSF1. (**E**) Relative levels of HSP mRNAs. Normalized levels of HSP mRNAs in undepleted cells treated with heat shock and restored for 1 h were arbitrarily set to 1.0; $n = 3$; $^{*}P < 0.05$; $^{**}P < 0.01$; n.s., not significant.

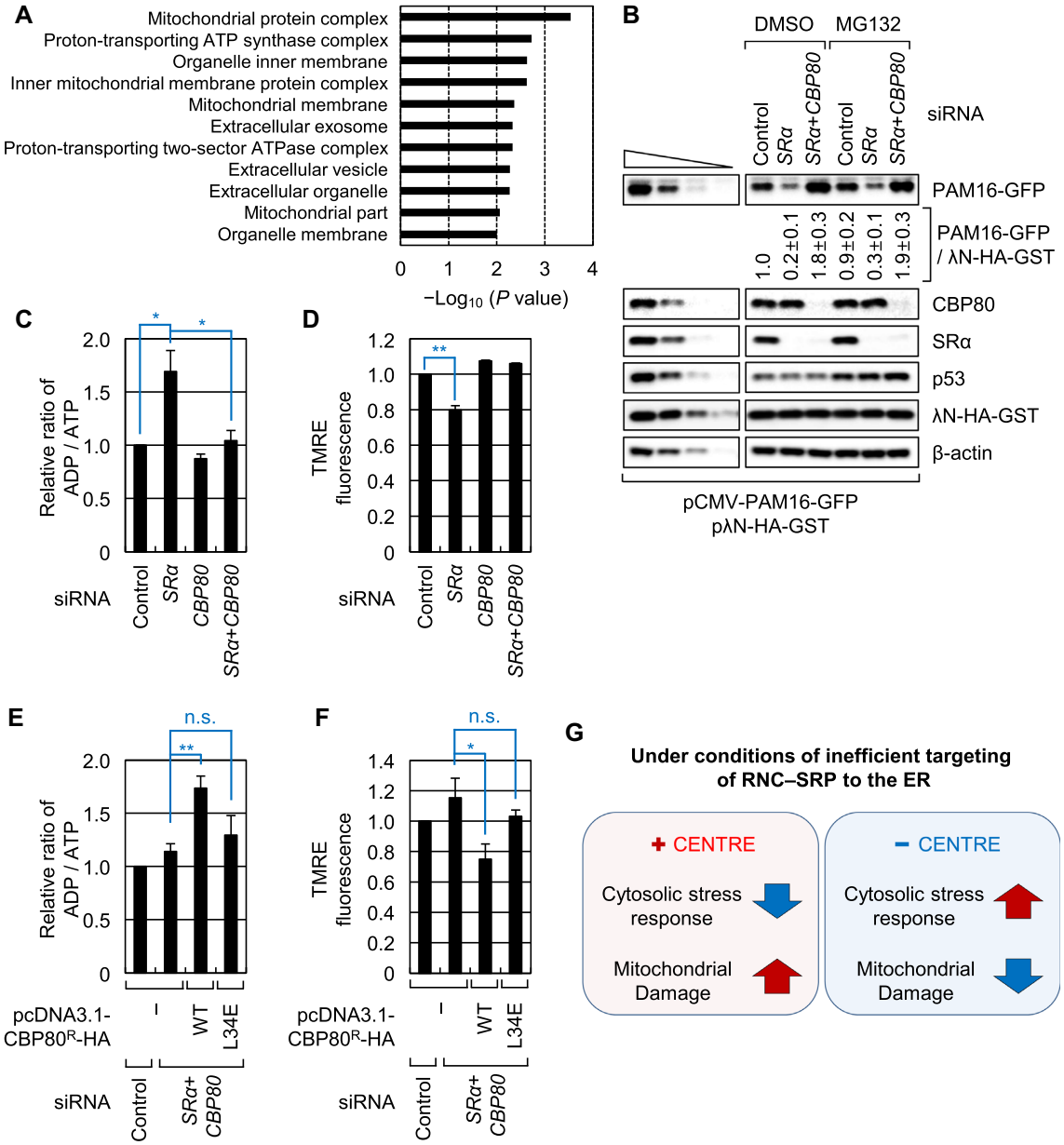

Figure 8. RNC–SRP misassembled on an mRNA coding for a mitochondrial protein is subject to CENTRE. (**A**) Gene ontology (GO) analysis of highly ranked transcripts (386; fold change ≥ 1.5) in Figure 2D, E. (**B**–**D**) Effects of single downregulation of SRα or double downregulation of both SRα and CBP80 on protein expression of PAM16-GFP mRNAs (panel B), intracellular ADP/ATP ratio (panel C), and mitochondrial membrane potential (panel D). TMRE, tetramethylrhodamine, ethyl ester. (**E** and **F**) Complementation using CBP80^{R}-WT or CBP80^{R}-L34E. Cells depleted of the indicated proteins were transiently expressed with siRNA-resistant CBP80^{R}-WT-HA or CBP80^{R}-L34E-HA. The intracellular ADP/ATP ratio (panel E) and mitochondrial membrane potential (panel F) were analyzed; $n = 3$; $^{*}P < 0.05$; $^{**}P < 0.01$; n.s., not significant. (**G**) Summary of the role of CENTRE during inefficient targeting of RNC–SRP to the ER.

The CENTRE pathway targets the RNC–SRP complex misassembled on an mRNA encoding a mitochondrial protein

As mentioned above, we proposed that CENTRE functions as a surveillance pathway that maintains CBC–RNC–SRP as a translationally inactive complex until it is properly delivered to the ER. To identify the major substrates subject to CENTRE, we performed Gene Ontology (GO) analysis of the 1533 mRNAs belonging to the CBP80 IP ∩ SRP68 IP group (Figure 2D, E, and Supplementary Table S3B). The set of mRNAs with the highest enrichment in the IP of CBP80 following SR downregulation included those associated with GO terms related to mitochondria (Figure 8A). Indeed, protein expression from highly ranked mRNAs associated with GO terms related to mitochondria (*PAM16*, *SLC25A41* and *ATP5E*) was significantly inhibited by SRα downregulation, but this was reversed by the double downregulation without affecting mRNA abundance (Figure 8B and Supplementary Figure S12). In agreement with the protein expression results, SRα downregulation led to both an increase in the ADP/ATP ratio (Fig-

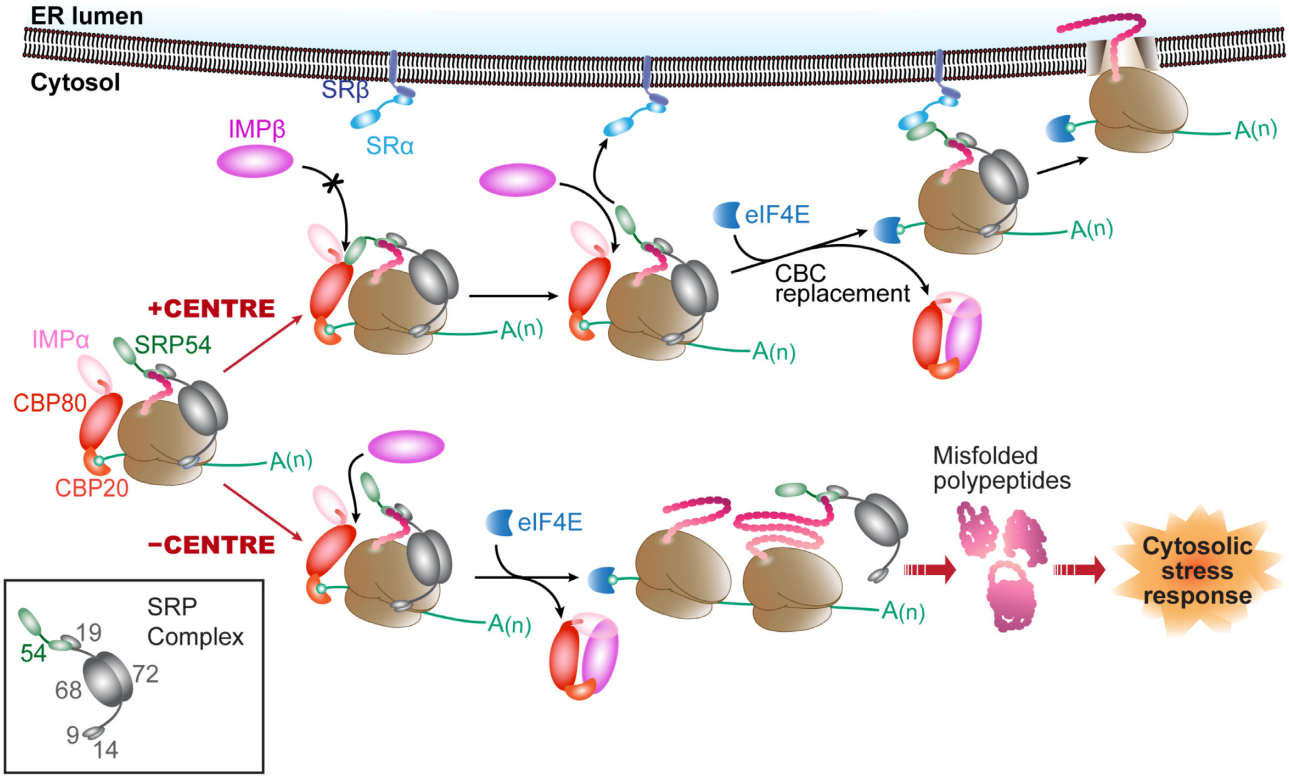

Figure 9. Proposed model of CENTRE. See the Discussion section for details.

ure 8C) and a decrease in membrane potential (Figure 8D), indicative of mitochondrial dysfunction. Notably, double downregulation restored mitochondrial function. This was reversed by complementation with CBP80^{R}-WT, but not with CBP80^{R}-L34E (Figure 8E and F). In addition, the intracellular distribution of PAM16-GFP protein largely overlapped with that of mitochondria (stained by MitoTracker) under normal conditions or conditions depleted of both SRα and CBP80 (Supplementary Figure S13). On the other hand, complementation with CBP80^{R}-WT, but not with CBP80^{R}-L34E, caused inappropriate intracellular distribution of PAM16-GFP. Given that signal sequences for ER and mitochondrial targeting share the N-terminal α-helical structure, but with different hydrophobicity levels (52), there may be non-specific interaction between SRP and the mitochondrial targeting sequence. Therefore, these results suggest that misassembled RNC–SRP on an mRNA encoding a mitochondrial protein is also translationally repressed by the CENTRE pathway when it is not efficiently targeted to the ER surface, resulting in mitochondrial dysfunction (Figure 8G).

DISCUSSION

Cellular proteins destined for the ER are subjected to rigorous quality control to ensure proper targeting of the proteins (2–4). As a nascent chain harboring a signal sequence exits a ribosome, the RNC is recognized and translationally arrested by an SRP. It resumes translation elongation on the surface of the ER only after the RNC–SRP complex is properly delivered to the ER. In contrast, when the signal sequence does not contain the sufficient number of hydrophobic residues, the mutated signal sequence fails to associate with the SRP. In this case, AGO2 binds to the mutated nascent chain and initiates rapid mRNA decay in a process called RAPP (19). Although RNC–SRP successfully passes RAPP, efficient translocation of the RNC–SRP complex is hampered by the intracellular concentration of the SR, which is known to be rate-limiting for ER targeting (17).

In this study, we unravel a co-translational quality control pathway, CENTRE, via which the CBC ensures strict maintenance of the RNC–SRP complex in a translationally-repressed, translocation-competent state until the RNC–SRP complex is properly delivered to the ER (Figure 9). When CENTRE is impaired or inefficient, IMPβ triggers promiscuous replacement of the CBC by eIF4E, even before the CBC–RNC–SRP complex is delivered to the ER. The resulting eIF4E–RNC–SRP complex synthesizes aberrant polypeptides at inappropriate cellular locations. Eventually, the accumulated aberrant and misfolded-polypeptide aggregates induce CSR, which is associated with many neurodegenerative pathologies, including Alzheimer's and Parkinson's diseases (14–16).

We also found that the CENTRE pathway targets a CBC–RNC–SRP complex misassembled on an mRNA encoding a mitochondrial protein (Figure 8). When the repressed complex reaches the ER surface, it is disassembled via a recently discovered surveillance mechanism, ER surface–mediated protein targeting (53). The released

mRNA can then be recycled in a new round of translation for proper mitochondrial targeting. In this way, during pioneer translation, CENTRE functions as a surveillance pathway that ensures proper targeting of proteins destined for the ER or mitochondria.

The tight regulation of the proper sorting of newly synthesized proteins into diverse membranous organelles and non-membranous structures is necessary for various cellular functions (5,54). Comprehensive elucidation of the mechanisms underlying subcellular localization of proteins is therefore crucial for a complete understanding of cell biology. In this study, we propose CENTRE as a quality control pathway specific for targeting to the ER or mitochondria. Molecular mechanisms involved in targeting proteins to other subcellular locations are likely to be under unique quality control systems which need to be investigated in future studies.

DATA AVAILABILITY

The next-generation sequencing and microarray data have been deposited in the Sequence Read Archive of the National Center for Biotechnology Information under accession number SRP194200 and in the Gene Expression Omnibus (GEO) data repository (series ID: GSE85795), respectively.

SUPPLEMENTARY DATA

Supplementary Data are available at NAR Online.

ACKNOWLEDGEMENTS

We thank Dr Andrey L. Karamyshev and Dr Philip J. Thomas for providing plasmids encoding either WT or Δ4L PPL, and Dr Lynne E. Maquat and Dr Narry V. Kim for their scientific comments.

FUNDING

National Research Foundation (NRF) of Korea grants funded by the Korean government (Ministry of Science, ICT and Future Planning) [NRF-2015R1A3A2033665 and NRF-2018R1A5A1024261]; Korea University Grant; J.P. was supported in part by an NRF grant funded by the Korea government (Ministry of Science, ICT and Future Planning) [NRF-2021R1C1C2013476]. Funding for open access charge: NRF [NRF-2015R1A3A2033665].
Conflict of interest statement. None declared.

REFERENCES

1. Aviram,N. and Schuldiner,M. (2017) Targeting and translocation of proteins to the endoplasmic reticulum at a glance. *J. Cell Sci.*, **130**, 4079–4085.
2. Kramer,G., Shiber,A. and Bukau,B. (2018) Mechanisms of cotranslational maturation of newly synthesized proteins. *Annu. Rev. Biochem.*, **88**, 337–364.
3. Zhang,X. and Shan,S.O. (2014) Fidelity of cotranslational protein targeting by the signal recognition particle. *Annu. Rev. Biophys.*, **43**, 381–408.
4. Akopian,D., Shen,K., Zhang,X. and Shan,S.O. (2013) Signal recognition particle: an essential protein-targeting machine. *Annu. Rev. Biochem.*, **82**, 693–721.
5. Pfanner,N., Warscheid,B. and Wiedemann,N. (2019) Mitochondrial proteins: from biogenesis to functional networks. *Nat. Rev. Mol. Cell Biol.*, **20**, 267–284.
6. Costa,E.A., Subramanian,K., Nunnari,J. and Weissman,J.S. (2018) Defining the physiological role of SRP in protein-targeting efficiency and specificity. *Science (New York, N.Y.)*, **359**, 689–692.
7. Phillips,B.P., Gomez-Navarro,N. and Miller,E.A. (2020) Protein quality control in the endoplasmic reticulum. *Curr. Opin. Cell Biol.*, **65**, 96–102.
8. Mercier,E., Holtkamp,W., Rodnina,M.V. and Wintermeyer,W. (2017) Signal recognition particle binds to translating ribosomes before emergence of a signal anchor sequence. *Nucleic Acids Res.*, **45**, 11858–11866.
9. Chartron,J.W., Hunt,K.C. and Frydman,J. (2016) Cotranslational signal-independent SRP preloading during membrane targeting. *Nature*, **536**, 224–228.
10. Schibich,D., Gloge,F., Pohner,I., Bjorkholm,P., Wade,R.C., von Heijne,G., Bukau,B. and Kramer,G. (2016) Global profiling of SRP interaction with nascent polypeptides. *Nature*, **536**, 219–223.
11. Rapoport,T.A., Li,L. and Park,E. (2017) Structural and Mechanistic Insights into Protein Translocation. *Annu. Rev. Cell Dev. Biol.*, **33**, 369–390.
12. Kobayashi,K., Jomaa,A., Lee,J.H., Chandrasekar,S., Boehringer,D., Shan,S.O. and Ban,N. (2018) Structure of a prehandover mammalian ribosomal SRP.SRP receptor targeting complex. *Science (New York, N.Y.)*, **360**, 323–327.
13. Sitron,C.S. and Brandman,O. (2020) Detection and degradation of stalled nascent chains via ribosome-associated quality control. *Annu. Rev. Biochem.*, **89**, 417–442.
14. Chin,L.S., Olzmann,J.A. and Li,L. (2010) Parkin-mediated ubiquitin signalling in aggresome formation and autophagy. *Biochem. Soc. Trans.*, **38**, 144–149.
15. Sontag,E.M., Samant,R.S. and Frydman,J. (2017) Mechanisms and functions of spatial protein quality control. *Annu. Rev. Biochem.*, **86**, 97–122.
16. Hipp,M.S., Kasturi,P. and Hartl,F.U. (2019) The proteostasis network and its decline in ageing. *Nat. Rev. Mol. Cell Biol.*, **20**, 421–435.
17. Lakkaraju,A.K., Mary,C., Scherrer,A., Johnson,A.E. and Strub,K. (2008) SRP keeps polypeptides translocation-competent by slowing translation to match limiting ER-targeting sites. *Cell*, **133**, 440–451.
18. Karamyshev,A.L. and Karamysheva,Z.N. (2018) Lost in translation: ribosome-associated mRNA and protein quality controls. *Front. Genet.*, **9**, 431.
19. Karamyshev,A.L., Patrick,A.E., Karamysheva,Z.N., Griesemer,D.S., Hudson,H., Tjon-Kon-Sang,S., Nilsson,I., Otto,H., Liu,Q., Rospert,S. *et al.* (2014) Inefficient SRP interaction with a nascent chain triggers a mRNA quality control pathway. *Cell*, **156**, 146–157.
20. Maquat,L.E., Tarn,W.Y. and Isken,O. (2010) The pioneer round of translation: features and functions. *Cell*, **142**, 368–374.
21. Ryu,I. and Kim,Y.K. (2017) Translation initiation mediated by nuclear cap-binding protein complex. *BMB Rep.*, **50**, 186–193.
22. Ishigaki,Y., Li,X., Serin,G. and Maquat,L.E. (2001) Evidence for a pioneer round of mRNA translation: mRNAs subject to nonsense-mediated decay in mammalian cells are bound by CBP80 and CBP20. *Cell*, **106**, 607–617.
23. Kim,Y.K. and Maquat,L.E. (2019) UPFront and center in RNA decay: UPF1 in nonsense-mediated mRNA decay and beyond. *RNA*, **25**, 407–422.
24. Kurosaki,T., Popp,M.W. and Maquat,L.E. (2019) Quality and quantity control of gene expression by nonsense-mediated mRNA decay. *Nat/ Rev. Mol. Cell Biol.*, **20**, 406–420.
25. Sato,H. and Maquat,L.E. (2009) Remodeling of the pioneer translation initiation complex involves translation and the karyopherin importin beta. *Genes Dev.*, **23**, 2537–2550.
26. Dias,S.M., Wilson,K.F., Rojas,K.S., Ambrosio,A.L. and Cerione,R.A. (2009) The molecular basis for the regulation of the cap-binding complex by the importins. *Nat. Struct. Mol. Biol.*, **16**, 930–937.
27. Jeong,K., Ryu,I., Park,J., Hwang,H.J., Ha,H., Park,Y., Oh,S.T. and Kim,Y.K. (2019) Staufen1 and UPF1 exert opposite actions on the replacement of the nuclear cap-binding complex by eIF4E at the 5' end of mRNAs. *Nucleic Acids Res.*, **47**, 9313–9328.

28. Cho,H., Han,S., Park,O.H. and Kim,Y.K. (2013) SMG1 regulates adipogenesis via targeting of staufen1-mediated mRNA decay. *Biochim. Biophys. Acta*, **1829**, 1276–1287.
29. Kim,K.M., Cho,H., Choi,K., Kim,J., Kim,B.W., Ko,Y.G., Jang,S.K. and Kim,Y.K. (2009) A new MIF4G domain-containing protein, CTIF, directs nuclear cap-binding protein CBP80/20-dependent translation. *Genes Dev.*, **23**, 2033–2045.
30. Nguyen,T.A., Jo,M.H., Choi,Y.G., Park,J., Kwon,S.C., Hohng,S., Kim,V.N. and Woo,J.S. (2015) Functional anatomy of the human microprocessor. *Cell*, **161**, 1374–1387.
31. Choe,J., Ryu,I., Park,O.H., Park,J., Cho,H., Yoo,J.S., Chi,S.W., Kim,M.K., Song,H.K. and Kim,Y.K. (2014) eIF4AIII enhances translation of nuclear cap-binding complex-bound mRNAs by promoting disruption of secondary structures in 5'UTR. *PNAS*, **111**, E4577–4586.
32. Park,J., Park,Y., Ryu,I., Choi,M.H., Lee,H.J., Oh,N., Kim,K., Kim,K.M., Choe,J., Lee,C. *et al.* (2017) Misfolded polypeptides are selectively recognized and transported toward aggresomes by a CED complex. *Nat. Commun.*, **8**, 15730.
33. Park,O.H., Ha,H., Lee,Y., Boo,S.H., Kwon,D.H., Song,H.K. and Kim,Y.K. (2019) Endoribonucleolytic cleavage of m(6)A-containing RNAs by RNase P/MRP complex. *Mol. Cell*, **74**, 494–507.
34. Ryu,I., Won,Y.S., Ha,H., Kim,E., Park,Y., Kim,M.K., Kwon,D.H., Choe,J., Song,H.K., Jung,H. *et al.* (2019) eIF4A3 phosphorylation by CDKs affects NMD during the cell cycle. *Cell Rep.*, **26**, 2126–2139.
35. Bustin,S.A., Benes,V., Garson,J.A., Hellemans,J., Huggett,J., Kubista,M., Mueller,R., Nolan,T., Pfaffl,M.W., Shipley,G.L. *et al.* (2009) The MIQE guidelines: minimum information for publication of quantitative real-time PCR experiments. *Clin. Chem.*, **55**, 611–622.
36. Cho,H., Kim,K.M., Han,S., Choe,J., Park,S.G., Choi,S.S. and Kim,Y.K. (2012) Staufen1-mediated mRNA decay functions in adipogenesis. *Mol. Cell*, **46**, 495–506.
37. Choe,J., Kim,K.M., Park,S., Lee,Y.K., Song,O.K., Kim,M.K., Lee,B.G., Song,H.K. and Kim,Y.K. (2013) Rapid degradation of replication-dependent histone mRNAs largely occurs on mRNAs bound by nuclear cap-binding proteins 80 and 20. *Nucleic Acids Res.*, **41**, 1307–1318.
38. Langmead,B. and Salzberg,S.L. (2012) Fast gapped-read alignment with Bowtie 2. *Nat. Methods*, **9**, 357–359.
39. Quinlan,A.R. and Hall,I.M. (2010) BEDTools: a flexible suite of utilities for comparing genomic features. *Bioinformatics*, **26**, 841–842.
40. Martin,M. (2011) Cutadapt removes adapter sequences from high-throughput sequencing reads. *EMBnet. J.*, **17**, 10–12.
41. Dobin,A., Davis,C.A., Schlesinger,F., Drenkow,J., Zaleski,C., Jha,S., Batut,P., Chaisson,M. and Gingeras,T.R. (2013) STAR: ultrafast universal RNA-seq aligner. *Bioinformatics*, **29**, 15–21.
42. Anders,S., Pyl,P.T. and Huber,W. (2015) HTSeq–a Python framework to work with high-throughput sequencing data. *Bioinformatics*, **31**, 166–169.
43. Huang da,W., Sherman,B.T. and Lempicki,R.A. (2009) Systematic and integrative analysis of large gene lists using DAVID bioinformatics resources. *Nat. Protoc.*, **4**, 44–57.
44. Huang da,W., Sherman,B.T. and Lempicki,R.A. (2009) Bioinformatics enrichment tools: paths toward the comprehensive functional analysis of large gene lists. *Nucleic Acids Res.*, **37**, 1–13.
45. Wild,K., Bange,G., Motiejunas,D., Kribelbauer,J., Hendricks,A., Segnitz,B., Wade,R.C. and Sinning,I. (2016) Structural basis for conserved regulation and adaptation of the signal recognition particle targeting complex. *J. Mol. Biol.*, **428**, 2880–2897.
46. Cho,H., Rambout,X., Gleghorn,M.L., Nguyen,P.Q.T., Phipps,C.R., Miyoshi,K., Myers,J.R., Kataoka,N., Fasan,R. and Maquat,L.E. (2018) Transcriptional coactivator PGC-1alpha contains a novel CBP80-binding motif that orchestrates efficient target gene expression. *Genes Dev.*, **32**, 555–567.
47. Tajima,S., Lauffer,L., Rath,V.L. and Walter,P. (1986) The signal recognition particle receptor is a complex that contains two distinct polypeptide chains. *J. Cell Biol.*, **103**, 1167–1178.
48. Miller,J.D., Tajima,S., Lauffer,L. and Walter,P. (1995) The beta subunit of the signal recognition particle receptor is a transmembrane GTPase that anchors the alpha subunit, a peripheral membrane GTPase, to the endoplasmic reticulum membrane. *J. Cell Biol.*, **128**, 273–282.
49. Cui,X.A., Zhang,H., Ilan,L., Liu,A.X., Kharchuk,I. and Palazzo,A.F. (2015) mRNA encoding Sec61beta, a tail-anchored protein, is localized on the endoplasmic reticulum. *J. Cell Sci.*, **128**, 3398–3410.
50. Ast,T., Cohen,G. and Schuldiner,M. (2013) A network of cytosolic factors targets SRP-independent proteins to the endoplasmic reticulum. *Cell*, **152**, 1134–1145.
51. Guettouche,T., Boellmann,F., Lane,W.S. and Voellmy,R. (2005) Analysis of phosphorylation of human heat shock factor 1 in cells experiencing a stress. *BMC Biochem.*, **6**, 4.
52. Kunze,M. and Berger,J. (2015) The similarity between N-terminal targeting signals for protein import into different organelles and its evolutionary relevance. *Front. Physiol.*, **6**, 259.
53. Hansen,K.G., Aviram,N., Laborenz,J., Bibi,C., Meyer,M., Spang,A., Schuldiner,M. and Herrmann,J.M. (2018) An ER surface retrieval pathway safeguards the import of mitochondrial membrane proteins in yeast. *Science (New York, N.Y.)*, **361**, 1118–1122.
54. Bauer,N.C., Doetsch,P.W. and Corbett,A.H. (2015) Mechanisms regulating protein localization. *Traffic*, **16**, 1039–1061.